

Carley Vuillermin and Sarah D. Bixby

---

## Overview of Imaging Modalities

### Radiographs

Plain radiographs are the first-line imaging modality for patients with suspected femoral fracture and are usually the only imaging modality needed for both diagnosis and treatment. Standard radiographic views of the femur include images in orthogonal projections, typically anteroposterior (AP) and lateral radiographs. Initial radiographs not only identify fractures, but also may suggest the presence of underlying pathologic lesions that may have predisposed the patient to fracture. The entire femur, including the hip and knee joints, should be imaged with orthogonal views. Disruptions to joints above and below the fracture with dislocation or subluxation are more common with certain fracture patterns and have implications for recommendations regarding further imaging. Scrutiny of the soft tissues for foreign body or soft tissue gas is

also important, as these signs may indicate an open injury or a soft tissue infection. Proper patient positioning is also important to evaluate for the degree of overriding of the fracture fragments, and the extent of fracture displacement and angulation. Specific types of radiographs will depend on the location of the fracture, and will be discussed in detail later on in the chapter.

### Computed Tomography (CT)

Computed tomography (CT) of the femur may be helpful for pre-operative planning for surgery on complex femoral fractures, or to further evaluate a possible pathologic lesion. Radiation doses will vary based on patient girth, field of view, tube current, image thickness, and amount of overlap between slices, among other factors. Each of these factors may be adjusted to minimize radiation dose. In general, lower-dose imaging protocols are the norm rather than the exception in pediatric imaging. In musculoskeletal imaging in particular, CT dose may be reduced significantly without sacrificing image quality, particularly when the indication for imaging is fracture. With current multi-detector row CT (MDCT) technology, thin-section axial datasets can be acquired quickly, with sub-millimeter slice thickness and spacing. These thin sections allow the data to be reformatted into other planes without additional radiation exposure. Reformatted images are often more helpful than axial data because the femur is

---

C. Vuillermin, MD  
Boston Children's Hospital, Boston, MA, USA

S.D. Bixby, MD (✉)  
Department of Radiology, Boston Children's Hospital,  
300 Longwood Avenue, Boston, MA 02115, USA  
e-mail: sarah.bixby@childrens.harvard.edu

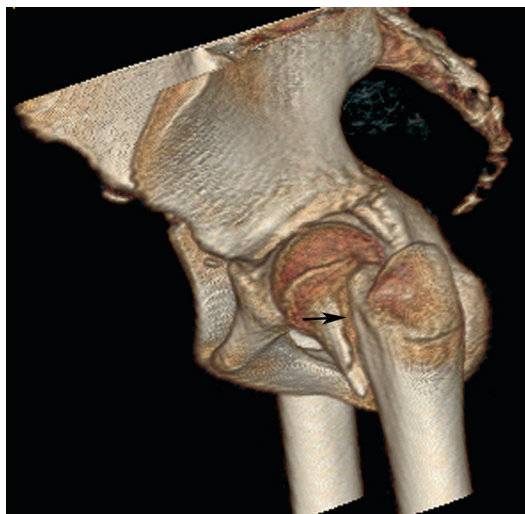


**Fig. 2.1** 3D reconstructed CT image of the pelvis using bone algorithm in an 11-year-old female s/p MVA demonstrates a left femoral neck fracture (*black arrow*) with mild posterior displacement of the femoral shaft with respect to the neck

projected in coronal and sagittal planes, which are comparable to radiographic views. MDCT with reformats accurately assess the degree of angulation and displacement of a femoral fracture in the coronal, sagittal, and transverse planes. The data may be used to create three-dimensional reconstructions of the fracture (Fig. 2.1), and may further identify and characterize a pathologic lesion (Fig. 2.2). CT does not require the use of intravenous contrast to evaluate the bony structures, but contrast may be necessary when there is concern for a vascular injury.

### Magnetic Resonance Imaging (MRI)

Indications for performing MRI of the femur depend on the type and location of fracture, and the risk of fracture complications. Magnet strengths vary by institution, though most imaging systems are 1.5 or 3.0 T. Dedicated extremity magnets with lower field strength magnets exist, though the hip and femur are not easily positioned within an extremity-only magnet. Higher field strength magnets are often preferred due to improved image resolution and decreased imag-

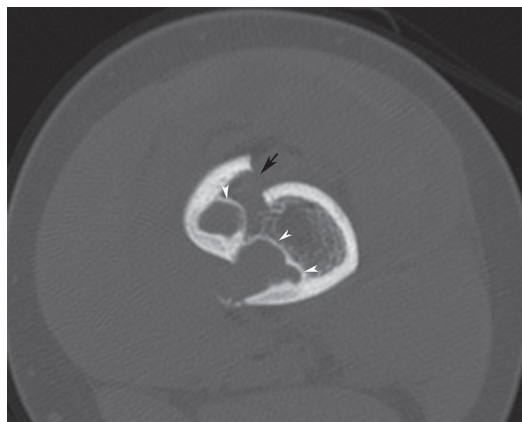


**Fig. 2.2** Axial image from a noncontrast CT scan of the femur in an 11-year-old boy demonstrates a fracture (*black arrow*) through a cortically based lesion with well-defined, sclerotic margins (*white arrowheads*), which represented a non-ossifying fibroma (NOF)

ing time relative to lower field strength systems. Coil selection and patient positioning in the coil are determined by the location of the fracture. Review of prior radiographs, if available, is critical for selecting the correct imaging coil and field of view for the examination. An MRI may require anywhere between 20 and 60 min of imaging time. Repeating sequences due to improper coil position or field of view selection may have a deleterious impact on the patient's ability to remain still, in addition to further delays for subsequent patients. Fractures of the proximal femur may be imaged with a surface coil placed over the affected hip, or a body/torso coil over the pelvis. Fractures involving the distal metaphysis or peri-physeal region, on the other hand, may be better evaluated using a dedicated knee coil. Though imaging protocols will vary depending on the specific indication for imaging, most protocols include fluid- and cartilage-sensitive sequences, as well as T1-weighted images to evaluate bone marrow signal. Fluid-sensitive sequences are often performed with fat suppression, which allows marrow and soft tissue edema to appear more conspicuous against the suppressed fat. T2-weighted sequences are fluid-sensitive and are often performed with chemical fat suppression. Cartilage-sensitive sequences include proton-density weighted sequences as well as gradient

echo sequences. Standard gradient echo sequences often have faster acquisition times compared to traditional spin-echo (e.g. T1, T2, Proton Density) sequences. There are also a variety of isotropic, thin-section, volumetric gradient echo sequences available today that allow for detailed evaluation of cartilage surfaces. Intravenous contrast may be required in cases of suspected avascular necrosis or infection, or if a pathologic lesion is suspected on prior imaging.

## Ultrasound

Ultrasound is rarely indicated in patients with femur fractures. One notable exception is pre-term neonates and infants with suspected physeal injuries and/or epiphyseal separations. The distal femoral epiphysis normally ossifies around 38 weeks' gestation, and the proximal femoral ossification center ossifies at around 4 months of age. In extremely young infants it may not be possible to detect the location of the femoral ossification center using radiographs. In these patients, ultrasound may be very helpful in imaging the cartilaginous epiphyses and detecting periosteal elevation and epiphyseal separation [1]. Specific findings of these injuries at ultrasound will be discussed further on the section on imaging young infants.

---

## Fracture Imaging Based on Location

Imaging of femoral trauma usually is directed by initial clinical assessment and mechanism of injury. Plain radiographs should focus on the primary region of interest, though it is also important to exclude associated injuries, including other fractures within the same bone, adjacent, or contralateral extremities [2]. Indications for advanced imaging modalities will be discussed in relation to imaging specific fracture types, as well as the section outlining the management of potential complications. In significantly displaced fractures, initial treatment should not be delayed pending advanced imaging where the additional imaging is unlikely

to change the primary management, and delay in treatment may compromise outcome.

## Proximal Femoral Fractures, Radiographic Evaluation, and AP Pelvis

Most fractures involving the proximal 1/3 of the femur will be diagnosed on the AP pelvis radiograph; this is part of a standard trauma imaging series. It is important not to use gonadal shielding as this may obscure key radiographic information. Ideally the limb will be in an approximate anatomic alignment in order to make interpretation more accurate; however, forceful movements should be avoided due to the risk of causing additional injury or causing significant discomfort to the patient. Assessment should be systematic, including both the bone and soft tissue elements. Cortical integrity should be assessed as well as the trabecular pattern. Subtle changes in trabecular orientation may be indicative of incomplete fractures. Shenton's line should be a smooth arc being created by the inferior aspect of the superior pubic ramus and the inferior aspect of the femoral neck. The femoral head should be concentric to the acetabulum. In small children this is hard to assess, as much of the acetabulum is a cartilage anlage, however it should be symmetric with the contralateral side. Small intra-articular gas bubbles may be seen on plain X-ray after a traumatic femoral head dislocation and subsequent reduction, however these are more readily appreciated on CT (Fig. 2.3). Soft tissue assessment includes evaluating for foreign material, calcifications, or gas indicative of possible open injuries. At times soft tissue creases can be mistaken for fracture lines, however they will extend beyond the cortical margins of the bone. Many fractures are readily diagnosed if there is a clear cortical disruption with either translation or angulation.

The AP pelvis radiograph changes significantly as a child matures and secondary centers of ossification appear and subsequently fuse (see Table 2.1 and Table 2.2). Skeletal maturity, in

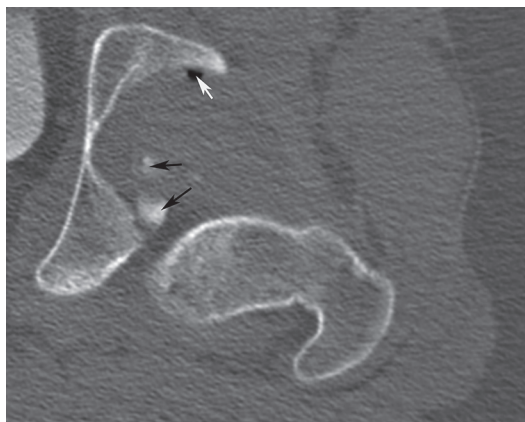


**Fig. 2.3** Axial CT image through the left hip from a CT of the abdomen and pelvis in an 18-year-old female s/p high speed MVA demonstrates posterior dislocation of the femur with at least two posterior acetabular wall fracture fragments projecting in the joint space (*black arrows*) and a small focus of gas within the joint (*white arrow*). This patient required surgical reduction of the hip with open reduction and fixation of the posterior wall fracture fragments

**Table 2.1** Normal timing of appearance of ossification centers [4]

Ossific nucleus	Age of ossification
Femoral head	4 months
Greater trochanter	3 years
Lesser trochanter	11–12 years

**Table 2.2** Normal timing of fusion of physes [3]

Physis	Age at closure (years)
Triradiate cartilage	12–14
Proximal femur	16–18
Greater trochanter	16–17
Lesser trochanter	16–17

particular the state of the physes, is critical in assisting selection of definitive management (Fig. 2.4a–c).

### Cross-Table Lateral

Once an intra-capsular fracture of the femoral neck has been diagnosed, it is important not to move the limb and risk disrupting the retinacular

blood supply any further. Cross-table (shoot-through) lateral radiographs of the femur can be performed without moving the affected leg. This is a cross-table view with the beam angled 45° to the table. The beam is centered on the femoral head or region of interest. This view can also be utilized for extra-capsular proximal femoral injuries. Once a bone is fractured then the proximal fragment will not necessarily move with distal limb repositioning, thereby limiting the information gained with the frog lateral. Limiting movement also minimizes the pain experienced by the child.

### Frog-Leg Lateral

In trauma the frog lateral is predominantly reserved for instances where no fracture has been seen on the AP radiograph and orthogonal views are needed to further assess the region and exclude fracture. This may be somewhat limited in the hip given that the greater trochanter may project over the femoral neck in an area of concern (Fig. 2.5a, b). The hip is flexed 30–40° and abducted 45°, bringing the proximal femur into lateral profile with an AP beam orientation. This view is not useful for additional characterization of acetabular pathology.

## Radiographic Classifications of Proximal Femoral Fractures

### Fracture Dislocations

Fracture dislocations of the proximal femur and hip joint are radiographically classified according to the Stewart Milford classification (Fig. 2.6) [5, 7]. Unlike in the adult these injuries are uncommonly associated with acetabular fractures [5]. Imaging in these fracture patterns is aimed at ensuring that the hip joint is reduced and that the reduction is concentric. Intra-articular fragments need to be specifically looked for and are best imaged via CT (Fig. 2.7). The size, location, and displacement of acetabular or femoral head fragments must be assessed (Fig. 2.8). The findings will dictate the manage-



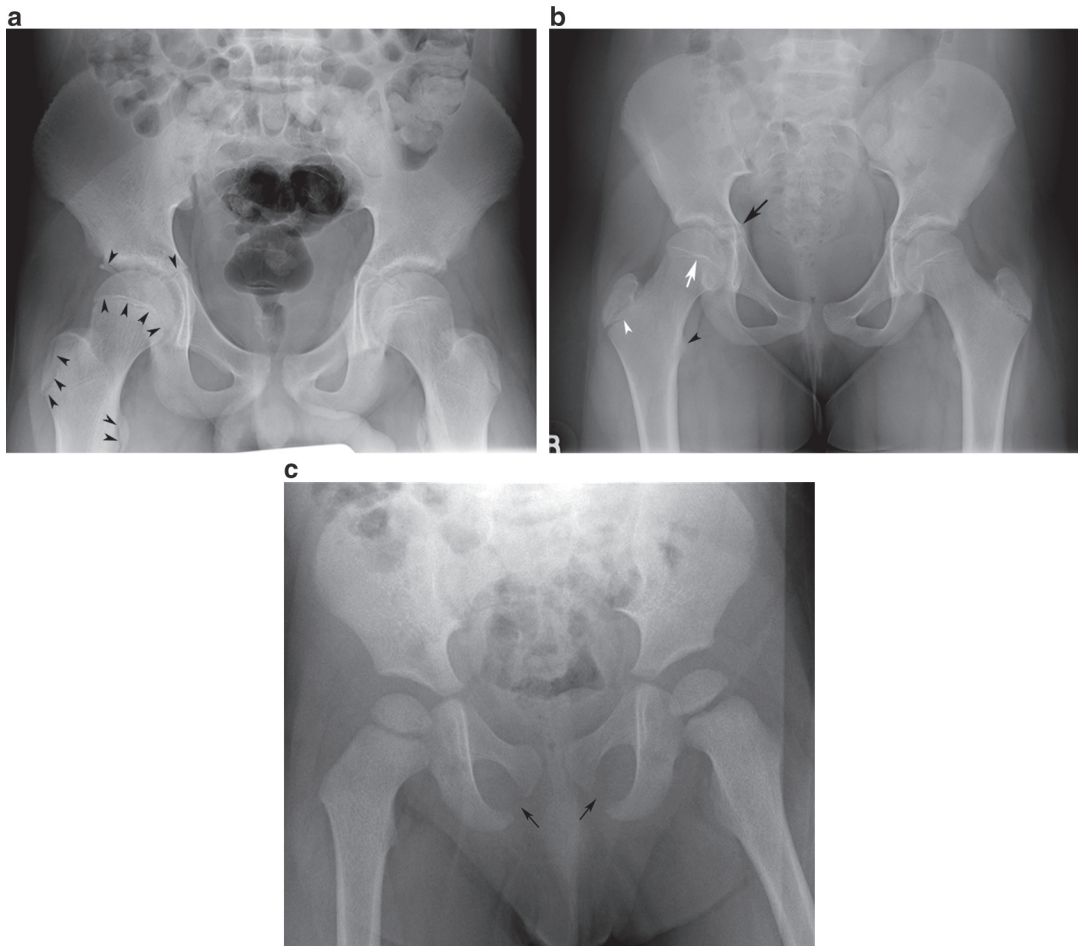


**Fig. 2.4** (a) AP radiograph of the pelvis in a 13-year-old male after car accident, demonstrates normal appearance of the open physes of the femoral heads, greater and lesser trochanters, triradiate cartilage, and acetabula (*black arrows*). This child sustained no pelvic or femoral fractures. (b) AP radiograph of the pelvis in a 10-year-old female demonstrates the normal appearance of the triradi-

ate cartilage (*black arrow*), proximal femoral physes (*white arrow*), greater trochanter (*white arrowhead*), and lesser trochanter (*black arrowhead*). (c) AP radiograph of the pelvis in a 20-month-old male after trauma demonstrates the normal appearance of the open physes of the pelvis and femur. Note the appearance of the unfused synchondroses (*black arrows*)

ment, including the operative approach. Femoral head fractures are classified according to the Pipkin Classification of femoral head fractures [8] (Fig. 2.9). It is important to remember that in children the osseous component may only represent a small proportion of the total fragment. Cross-sectional imaging is also essential as a standard post-reduction step to confirm concentric reduction and the absence of intra-articular fragments, with MRI having the advantage of elucidating size and position of chondral fragments (Fig. 2.10a–c) [6].

Femoral neck fractures are classified according to the radiographic classification of Delbet [9] (Fig. 2.11). In pediatric hip fractures this has been shown to be prognostic, especially in the development of AVN [10]. If suspicion arises for possible intra-articular fragments, including widening of the joint space without fragment visible, or an acetabular rim fracture or femoral head fracture is seen on plain radiographs, then patients should undergo CT scanning. CT is the preferred imaging modality as it is better at characterizing the size and location of bony fragments. If clini-

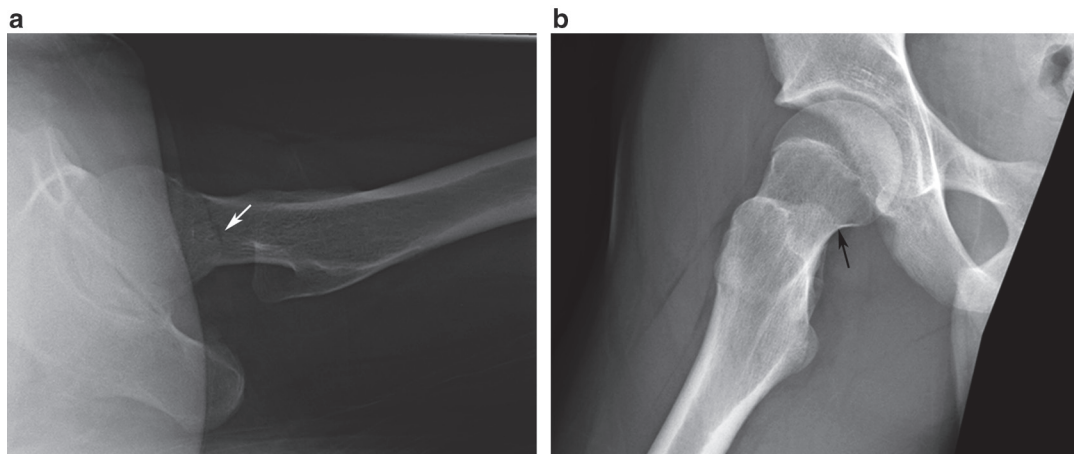


**Fig. 2.5** (a) Cross-table lateral radiograph of the left femur in a 15-year-old female s/p fall demonstrates a fracture through the femoral neck (*white arrow*). (b) Frog-leg lateral radiograph of the right hip in a 15-year-old male

with a stress fracture through the inferomedial femoral neck (*black arrow*) partially obscured by the overlying greater trochanter

cal suspicion remains for a fracture of the proximal femur and plain radiographs are negative, then MRI is the imaging modality of choice. MRI has been shown to be more sensitive than CT in detecting nondisplaced femoral neck fractures [11] (Fig. 2.12a, b). It can also be utilized for imaging possible physeal separations in younger children, where a chondral lesion may be contributing to a failure of concentric reduction following dislocation, or for assessing the size of a posterior wall fragment in fracture dislocations [12]. Femoral neck fractures are characterized by the location of the fracture within the neck, including subcapital (Fig. 2.13), transcervical (Fig. 2.14), cervicotrochanteric, and pertrochanteric (Fig. 2.15a, b).

### Physeal Fractures

Physeal fractures of the proximal femur are less frequent than distal femoral physeal injuries. The most common physeal injury of the proximal femur is slipped capital femoral epiphysis (SCFE). Although trauma may be part of the presentation in SCFE, it is generally considered a primary hip condition rather than a femur fracture, as there are other factors in addition to trauma that predispose patients to SCFE including obesity and endocrine disorders, as well as the shape of the acetabulum [13]. SCFE is most

often diagnosed on the basis of pelvic radiographs. Traumatic epiphyseal separation of the proximal femur is a rare injury that may occur after high-impact trauma, such as a fall from a height or a high-speed motor vehicle collision. The femoral head is often completely dislocated from the acetabulum. These fractures are diagnosed on the basis of radiographs, and CT imaging with 3D reconstructions may be performed to better define the spatial relationship between the femoral head, neck, and acetabulum. These fractures are catastrophic injuries with a high rate of avascular necrosis (>80 %) even after treatment [14] (Fig. 2.16a, b).

### Femoral Shaft

#### AP and Lateral Femoral Radiographs

For suspected femoral shaft fractures, initial views of the femur are obtained with the limb in approximate anatomic alignment. Ideally the entire femur will be imaged on a single radiographic plate (Fig. 2.17). Standard radiographic plates are up to 14 in. × 17 in. Placing the plate obliquely will increase the available length (Fig. 2.18). Consideration may be given to using a long plate (3 ft, stitched film) or it may be necessary to use two separate radiographs to ensure that the entire

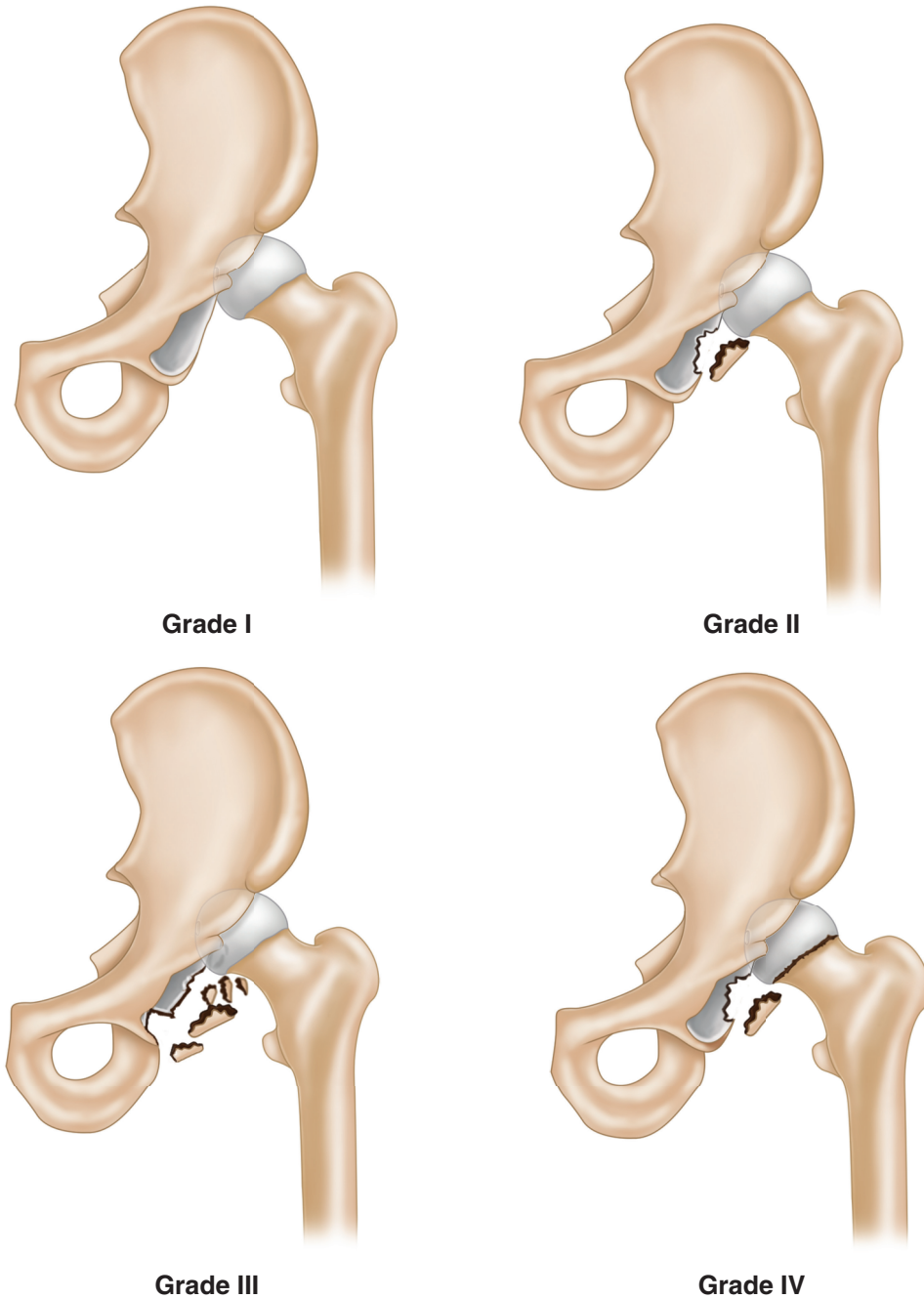


**Fig. 2.6** Illustration demonstrating the Stewart Milford classification of hip fracture/dislocations

femur, including the joints above and below, are imaged. Assessment of the film should include the fracture pattern, classified according to the AO classification (Fig. 2.19). Specific features to

note include the degree of displacement and angulation, the anatomic location (either proximal, middle or distal third of the diaphysis), the inner canal diameter on both the AP and lateral

**Fig. 2.7** Coronal reformatted image from a noncontrast CT scan of the pelvis in a 12-year-old male s/p ski injury with a crescentic fragment projecting in the right hip joint inferior to the fovea (*black arrow*), which represented an avulsed fragment from the femoral head (Pipkin type 1 fracture)

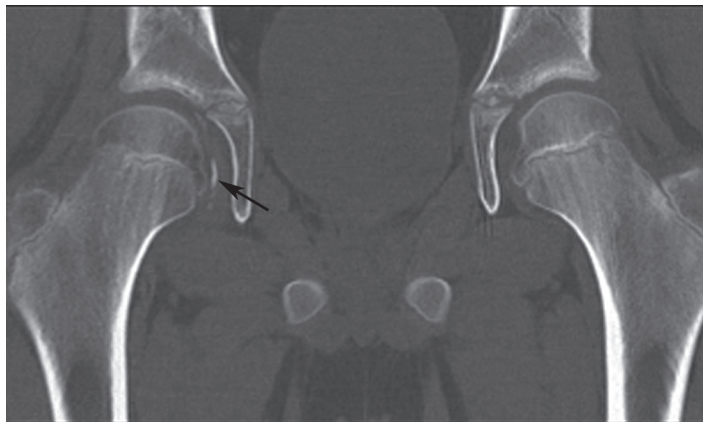


**Fig. 2.8** Coronal reformatted CT image through the left hip in a 18-year-old female s/p high-speed MVA demonstrates Grade III fracture/dislocation injury according to Steward Milford classification. There is widening of the medial joint space secondary to two posterior acetabular wall fracture fragments projecting in the joint space (*black arrows*) and a nondisplaced fracture through the medial wall of the acetabulum (*black arrowhead*). This required surgical dislocation for removal of the loose bodies

radiographs, and the skeletal maturity of the patient. In addition, it is important to assess the soft tissues to look for defects, gas, or foreign material (Fig. 2.20). Each of these factors will assist in management decision-making.

### Associated Injuries

Femoral shaft fractures are predominantly high-energy injuries. They are associated with ipsilateral proximal [2, 15] and distal femoral fractures,

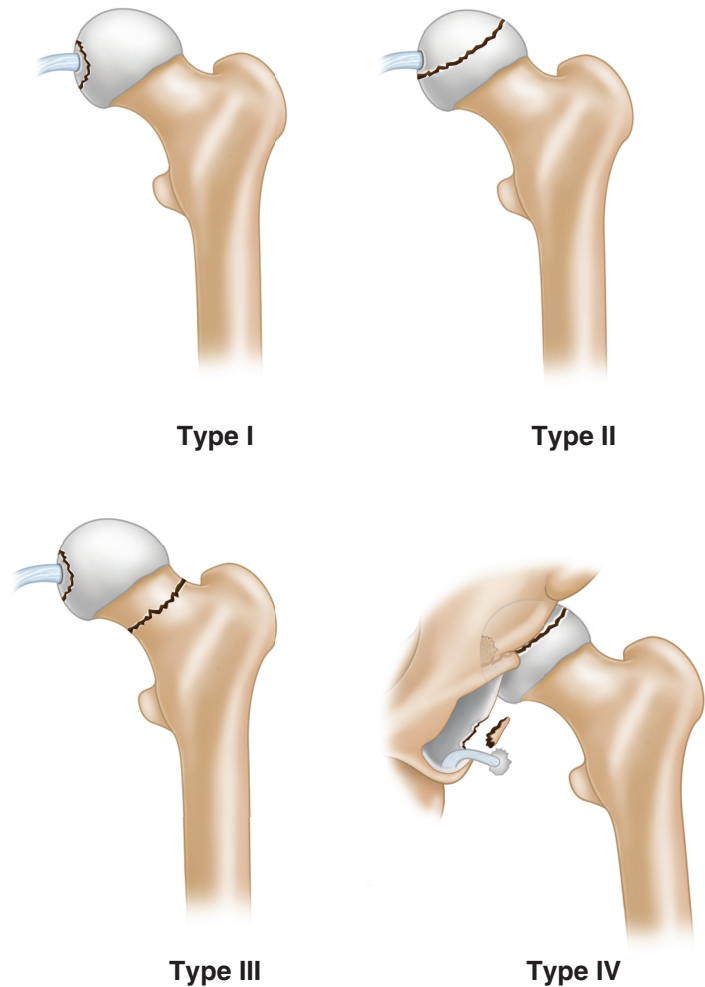
dislocations of adjacent joints, ligamentous and meniscal injuries of the knee [16], as well as proximal tibial [17] and pelvic fractures. In general, management of long bone fractures should not be delayed pending MR scanning to assess soft tissue injuries, especially in the setting of vascular injury.

## Distal Femoral Fractures

### Physeal Fractures

Fractures of the distal femoral growth plate are common in children, as the physeal cartilage is weaker than surrounding bones and ligaments. The physis is involved in 15–30% of all long bone fractures in children [18]. The most widely used classification scheme for growth plate fractures is the Salter-Harris classification system, which is based on the extent of involvement of the physis, metaphysis, and epiphysis [19] (Fig. 2.21). Salter 2 is the most common type of physeal fracture [20–22] and consists of a fracture through both the physeal plate and the metaphysis. The metaphyseal fragment may be easily detected if there is significant displacement of the fragment, though these fractures may be subtle on radiographs if little to no displacement has occurred (Fig. 2.22a, b). Salter 3 and Salter 4 fracture through the femoral condyles are rare injuries, usually related to a high-energy traumatic event [23]. These fractures extend to the articular surface of the femoral condyle, a finding that may be subtle on radiographs but

**Fig. 2.9** Pipkin classification of femoral head fractures



well depicted with CT. CT is also helpful for identifying “Hoffa fractures,” the coronal plane fracture within the lateral femoral condyle. Initial radiographic classification of a fracture is often modified after MRI [24] when subtle epiphyseal or metaphyseal fracture lines are detected. For these reasons, it is not uncommon for a patient with a known or suspected fracture in the region of the distal femoral physis to undergo further cross-sectional imaging (Fig. 2.23a, b).

Systematic review of any MRI of the knee in a patient with a traumatic injury and equivocal or negative radiographic findings should include scrutinizing the physes for widening, epiphyseal or metaphyseal fracture lines, bone marrow edema, and periosteal elevation [25]. Additional

advantages of MRI in evaluating fractures around the physis include the ability to evaluate for additional internal derangement of the knee, including cruciate or collateral ligament injuries, chondral injuries, and meniscal tears. MRI in patients with known or suspected distal femoral physeal injury may be performed with a dedicated knee coil. Standard T1, PD, and T2-weighted spin-echo sequences are usually sufficient to identify and characterize the fracture (Fig. 2.24a, b). Images should be acquired in all three imaging planes (axial, coronal, and sagittal) to fully characterize the fracture in each plane. With modern imaging sequences this may be performed with one volumetric, 3D sequence, ideally with proton density weighting which can be reformatted into different



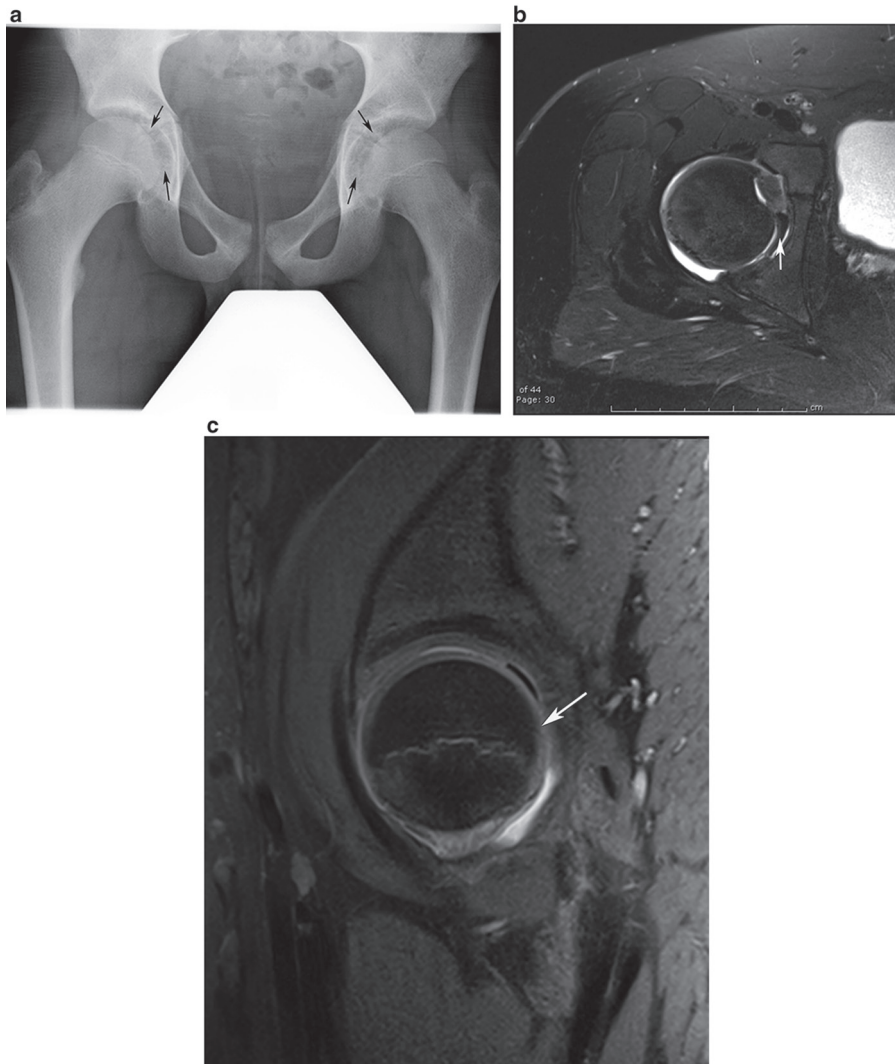


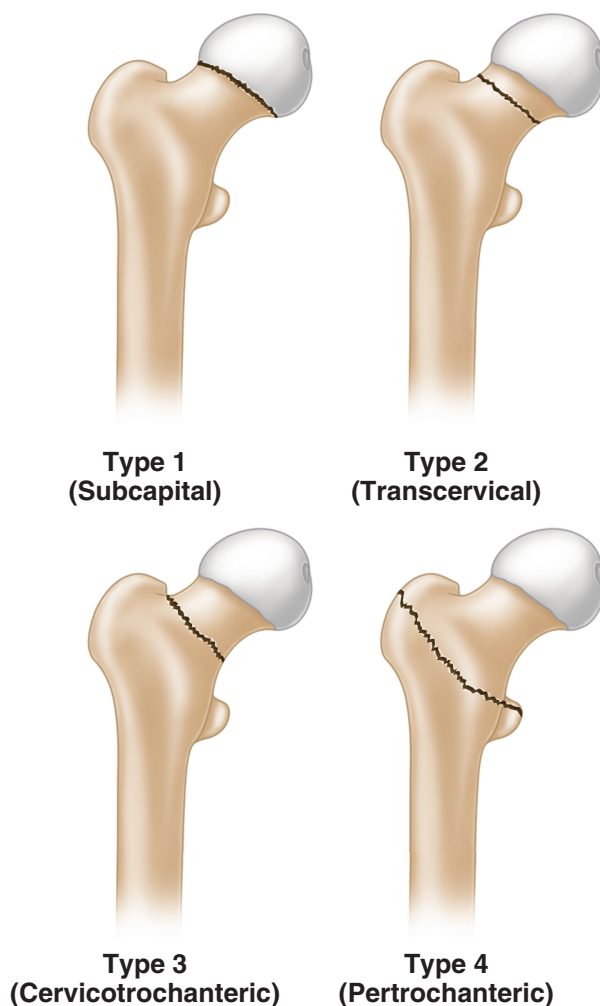
**Fig. 2.10** (a) AP radiograph of the pelvis in a 15-year-old male s/p MVA demonstrates relative widening of the left hip joint space compared to the right (*black arrows*) consistent with nonconcentric reduction. Subsequent MRI revealed entrapment of the posterior labrum within the central joint space on the left side. (b) Axial T2-weighted image with fat suppression in a different 12-year-old male

after hip dislocation/relocation demonstrates a flipped posterior labrum in the joint space (*white arrow*). The ligamentum teres has also avulsed from the femoral head. (c) Sagittal proton density-weighted image with fat suppression in a 12-year-old male after hip dislocation/relocation demonstrates a flipped posterior labrum in the joint space (*white arrow*)

planes. One T1-weighted sequence (most often in the coronal plane) is preferred for evaluating the marrow signal and demonstrating linear, low-signal intensity fracture lines. T2-weighted images with fat suppression reveal the surrounding marrow edema and fluid signal within the involved portions of the physis. On fluid-sensitive sequences, the physis should appear as a band of

bright signal between the low signal intensity epiphyseal plate and zone of provisional calcification [18] (Fig. 2.25). Interruption of the physis manifests as an area of low signal intensity within the physis on fat-suppressed water-sensitive sequences [18] (Fig. 2.26). It is not uncommon to see small “tongues” of physal cartilage extending into the metaphysis after a Salter-Harris

**Fig. 2.11** Illustration demonstrating the Delbet classification of femoral neck fractures



injury. These physal cartilage irregularities are likely related to a traumatic vascular insult [26], but are not usually associated with growth disturbance. Disruption of the periosteum may also be detected at MRI. When periosteal stripping or disruption is detected at MRI, careful attention should be given to the periphery of the physis to ensure that the stripped periosteum is not entrapped within the physis (Fig. 2.27).

### Subarticular Fractures

The term “bone bruise” is often used to describe an area of marrow edema (bright signal on fat-suppressed, fluid-sensitive sequences) in patients

with a known trauma history. A traumatic impaction injury may lead to various types of subcortical contusions and fractures depending on the precise mechanism. Vellet et al. described five subcortical fracture patterns, all of which demonstrated decreased T1-weighted signal and increased T2-weighted signal on MRI images [27]. Most of these injuries are occult on radiographs. Reticular fractures are areas of reticular stranding and signal abnormality within the marrow distant from the cortical bone. Geographic fractures are contiguous with the cortical bone. Linear fractures are discrete, linear areas of signal abnormality usually less than 2 mm wide (Fig. 2.28). Impaction fractures occur in conjunction with geographic or reticular fractures, and demonstrate variable

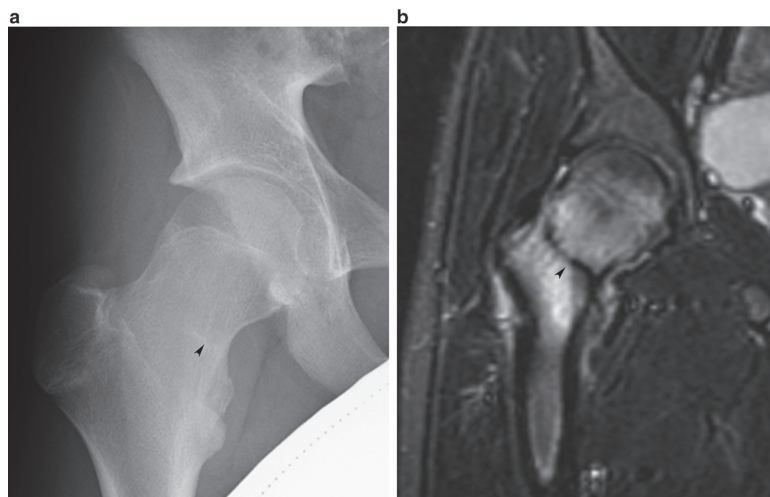


**Fig. 2.12** (a) AP radiograph of the right hip in a 15-year-old cross-country runner with right hip pain demonstrates a subtle, thin, linear sclerotic band along the inferior femoral neck perpendicular to the trabecular markings (*black arrowhead*). (b) Coronal T2-weighted MRI image fat-

suppressed image of the right hip in the same 15-year-old male runner demonstrates a dark linear fracture line at the inferior margin of the right femoral neck which is perpendicular to the trabecular markings (*black arrowhead*), with surrounding marrow edema



**Fig. 2.13** Frog-leg lateral radiograph of the left femur in a 20-month-old male s/p trauma demonstrates posterior displacement and angulation of the femoral head and widening of the physis, consistent with a Delbet Type I fracture

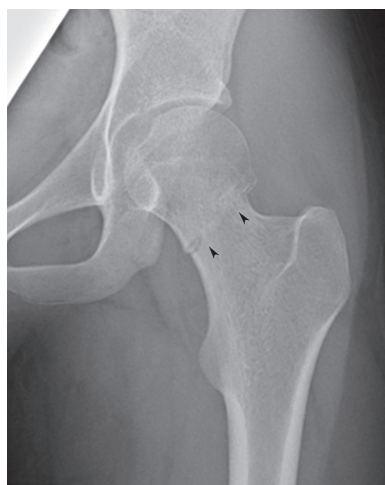


**Fig. 2.14** AP radiograph of the right hip in a 15-year-old female figure skater after fall demonstrates a transcervical femoral neck fracture consistent with a Delbet Type II fracture (*black arrowheads*)

degrees of depression of the articular surface. Osteochondral fractures are discrete cortical fractures circumscribing an area of subcortical marrow fat with an intact articular surface [27]. While this precise classification system is not used in common practice, the presence of subcortical injury is important to recognize because it may

have important short- and long-term prognostic implications for the patients. The correct identification of the fracture may provide an explanation for the patient's symptoms in the short term, and may also help guide appropriate treatment in order to avoid best outcome in terms of overlying chondral integrity in the long term [27].

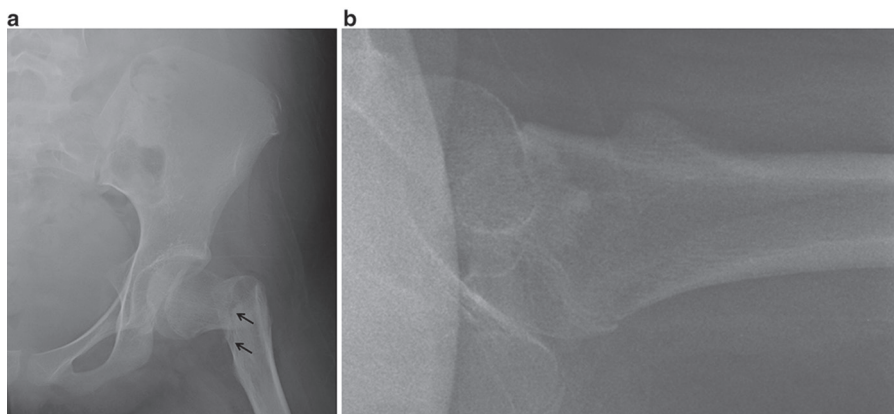


**Fig. 2.15** (a) AP radiograph of the left hip in a 12-year-old female demonstrates a fracture through the cervicotrochanteric portion of the femoral neck. (b) Lateral

radiograph of the left hip in a 12-year-old female demonstrates a fracture through the cervicotrochanteric portion of the femoral neck

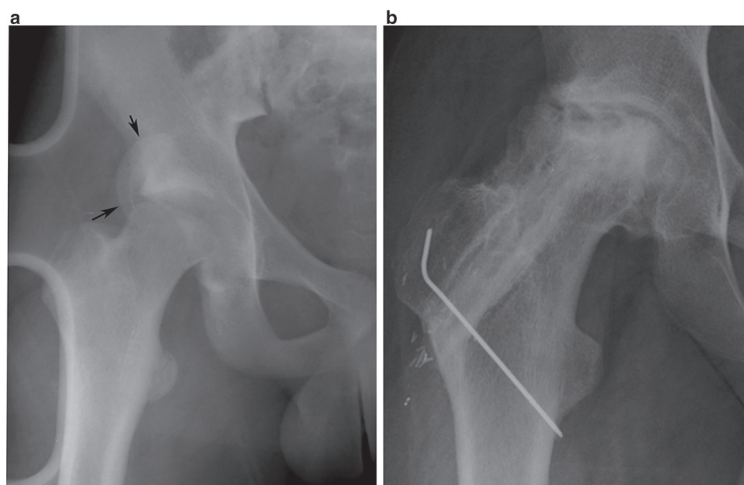


**Fig. 2.16** (a) AP radiograph of the pelvis in a 14-year-old male s/p MVA demonstrates traumatic epiphyseal separation of the right femoral head (black arrows) from the femoral neck, with posterior displacement and lateral rotation of the head with respect to the acetabulum. (b) AP radiograph of the pelvis in a 14-year-old male s/p MVA 4

years after injury demonstrates sclerosis, fragmentation, and collapse of the femoral head with joint space narrowing and degenerative changes, consistent with end-stage avascular necrosis. Post-surgical changes related to prior fibular graft are noted within the femoral neck

## Radiographically Occult Fractures

Most femur fractures are detected at plain radiography. Equivocal findings should prompt additional views, such as oblique and/or cross-table lateral radiographs. Even with additional views, approximately 2% of pediatric femoral fractures

will have no radiographic abnormality [28]. Most will be subarticular injuries or Salter-Harris fractures [19], which are well appreciated with MRI. MRI should, therefore, be considered in a child with persistent thigh or knee pain after injury to evaluate for occult fracture or other soft tissue abnormality.

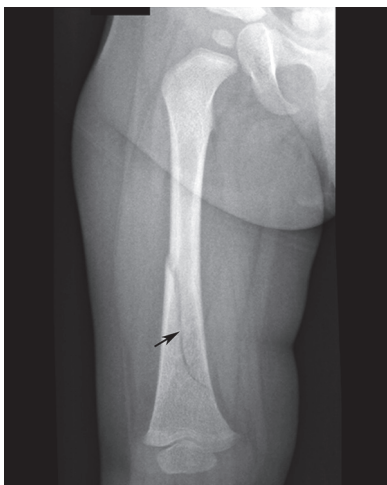


**Fig. 2.17** AP radiograph of the entire right femur in a 12-month-old male demonstrates an obliquely oriented fracture through the mid to lower shaft of the femur (*black arrow*)



**Fig. 2.18** Lateral radiograph of the femur in a 6-year-old male s/p MVA demonstrates a comminuted fracture through the midshaft of the left femur with anterior angulation of the distal fracture fragment and an anteriorly positioned, overlapping fragment (*black arrow*)

## Imaging of Fractures in Infants and Neonates

Femur fractures in infants and neonates are uncommon, mainly because these patients are nonambulatory [29]. Fractures in children under the age of 2 years, particularly those children who are not yet walking, are highly suspicious of child abuse [29–31]. Patients younger than 18 months old with femur fractures are more likely to be victims of abuse than accidental trauma [32]. If a non-ambulatory child presents with a femur fracture, a careful history should be elicited to determine if the mechanism put forth could reasonably explain the injury.

Metaphyseal irregularities and periosteal new bone formation are the most common signs of injuries to the long bones of abused infants [33]. The classic metaphyseal lesion (CML) was originally described by Dr. Caffey in 1957 [34] and is a high-specificity indicator of abuse [35]. The distal femur and proximal tibia are the most common sites for the classic metaphyseal lesion in abused infants [36]. This type of injury is a planar fracture through the bone rather than a circumferential fracture, giving rise to various imaging appearances. A “corner fracture” appearance of

the CML will be visible with a triangular, peripheral metaphyseal component of the fracture projects tangentially (Fig. 2.29), whereas the fracture will have a more “bucket-handle” configuration if the knee is flexed and the fragment projects at an obliquity [33] (Fig. 2.30). Given the subtlety of these particular fractures, radiographs should be performed with high-detail imaging systems when such a fracture is suspected, with careful attention directed to the metaphyses.

Injuries to the proximal femoral physis in the non-ambulatory child are less common than distal epiphyseal injuries, but also highly correlated with abuse [37] (Fig. 2.31). However, infants may sustain a proximal femoral epiphyseal injury as a result of birth trauma. In these rare instances, if history of difficult delivery is not provided, and the healing response is not appropriate for a birth injury, abuse must be considered. Plain radiographs in the acute stage may not demonstrate the fracture, given that the femoral head is not yet ossified in infants younger than 4 months.

In infants with a proximal femoral epiphyseal separation type of injury, radiographs may be misinterpreted as developmental hip dysplasia (DDH) if the femoral shaft is not aligned with the acetabulum. Ultrasound is helpful in differentiating fracture



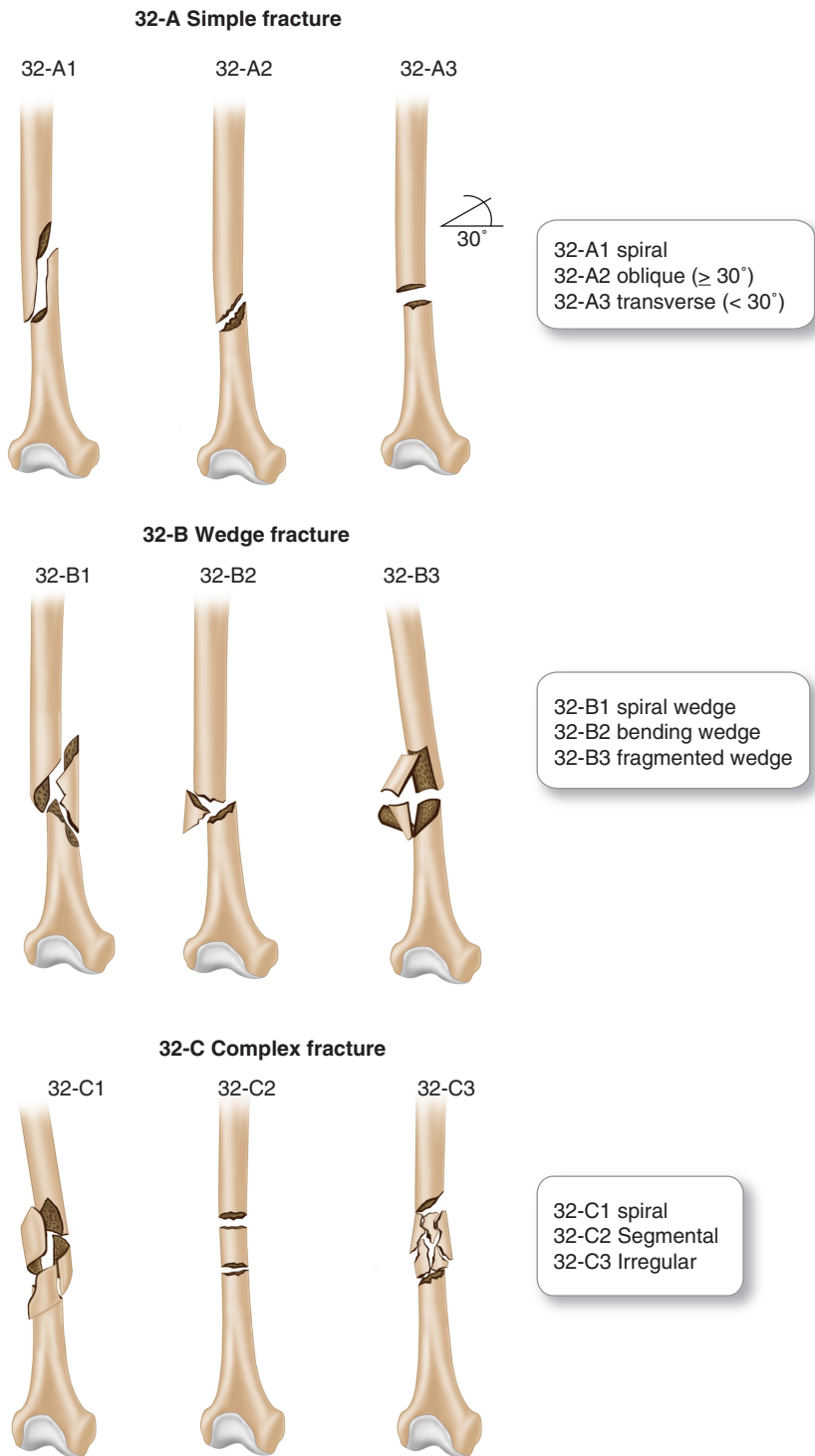


**Fig. 2.19** AO classification of femoral shaft fractures



**Fig. 2.20** AP radiograph of the right femur in a 16-year-old male s/p MVA demonstrates a comminuted fracture through the distal shaft of the femur as well as several punctate foci of gas within the soft tissues (*white arrows*), indicating an open injury

from dislocation by demonstrating the non-ossified femoral head within the acetabulum. Another benefit of ultrasound is identifying fractures at or near the growth plate in infants and neonates, including epiphyseal separation injuries. With ultrasound, the bone may be imaged in a circumferential fashion, whereas with radiographs two orthogonal views are often all that are available. Subtle growth plate injuries or metaphyseal fractures may be detected with ultrasound (Fig. 2.32). Soft tissue thickening and edema is often seen alongside osseous fractures at ultrasound. As the fracture begins to heal, radiographs become much more helpful in identifying the injury and evaluating healing and alignment. Once the proximal and distal femoral ossification centers have begun to ossify, ultrasound is rarely indicated in the evaluation of femoral fractures.

## Imaging Findings Associated with Complications of Pediatric Femur Fractures

### Nonunion and the Assessment of Union

Nonunion in pediatric fractures is rare. In a series of 43 pediatric fracture nonunions at a

level I trauma center over a 15-year period, only 2 were in the femur [39]. Fracture healing assessment, however, is critical in determining the management of all patients following femoral fractures. Although conceptually simple, the working definitions of union and nonunion in the pediatric population vary between clinicians [40, 41].

Assessment of radiographic union most commonly starts with orthogonal conventional radiographs that allows for qualitative assessment of callus formation, loss of fracture line visibility, cortical bridging, and restoration of trabecular bridging (Fig. 2.33). Radiographic union has classically been defined as three out of four cortices demonstrating bony bridging. When there is uncertainty, then oblique radiographs may assist with visualization of the fracture line, which is especially true if the fracture line is in an oblique plane or fixation hardware obstructs visualization in traditional views. While assessment of cortical bridging has been shown to be the most reliable indicator of union [42], this feature may correlate poorly with mechanical strength [43, 44].

When uncertainty persists regarding fracture union, CT is the imaging modality of choice. MDCT has been shown to be more accurate in detecting the extent of healing around orthopedic implants [45]. Hardware density, thickness, shape, and orientation to the gantry affect the degree of artifact generated, as do the scanner properties and post-processing algorithm applied. Settings can be altered to minimize artifact, including slice thickness and pitch, and post-processing techniques may also be employed to reduce artifact (Fig. 2.34a–c) [46].

### Implant Failure

When implants are used to stabilize a fracture, during the early healing process there is a balance between the development of union and the potential development of prosthetic and periprosthetic complications. Although clinical features often arise after a complication has occurred, subtle radiographic signs of an impending complication may precede the clinical presentation and are important

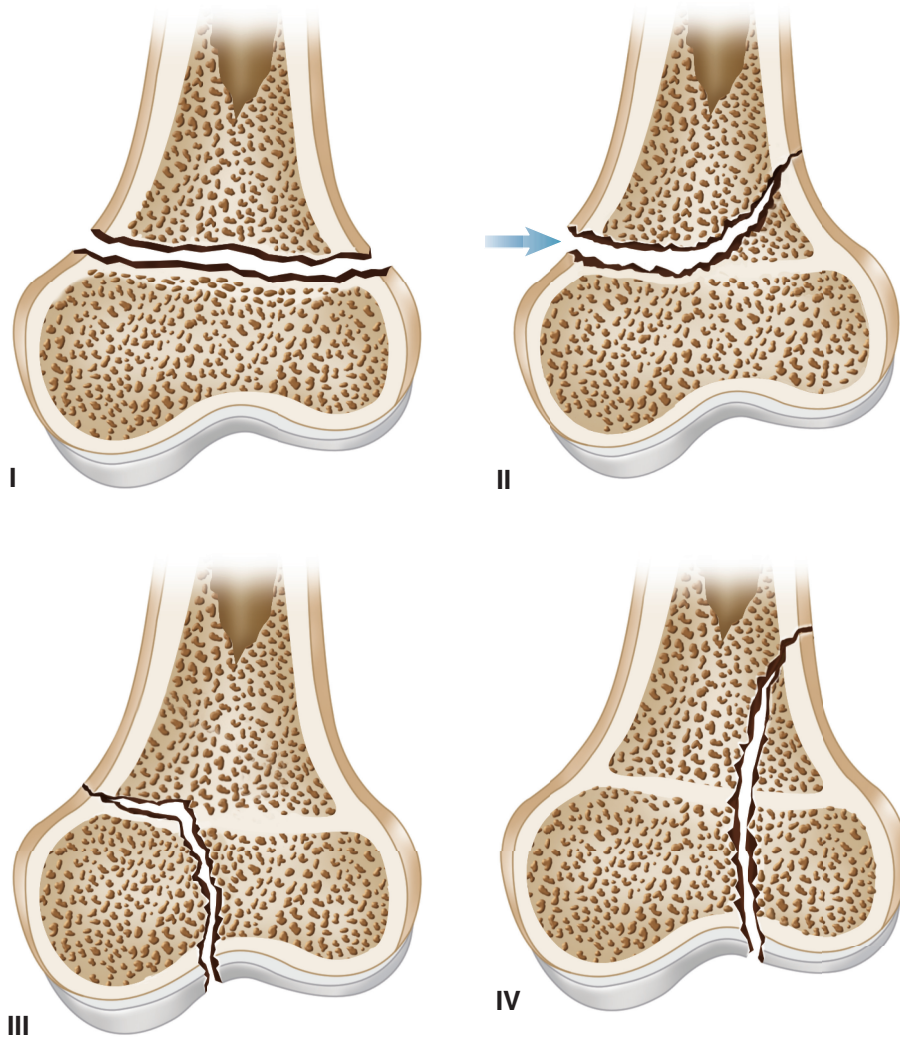


**Fig. 2.21** Illustration demonstrating the Salter-Harris classification of physeal fractures

to detect, if possible. Serial radiographs may show changes in fracture alignment or implant position, overt fracture of the implant, or loss of fixation. Where implant motion occurs, radiographic lucencies may develop around screws, which are referred to as halos. Where substantial motion is occurring then an effect called “windshield-wiper” occurs, in which the lucency is wider at the ends where maximal motion is occurring.

Implant fracture occurs when microstructural damage progresses to cyclical loading, then cracking, and finally crack propagation.

Radiographic signs that may indicate imminent failure of a plate, rod, or screw includes angular changes within the implant, or ultimately a discrete fracture line within the implant (Fig. 2.35).

Although plain radiographs commonly yield the required information, it has been shown that CT is more sensitive in detecting hardware-related complications [45, 47, 48]. MR is not a preferred modality, as the majorities of orthopedic implants are ferromagnetic and result in substantial artifact without yielding useful clinical information regarding the integrity of the hardware.

**Fig. 2.22** (a) AP radiograph of the knee in a 15-year-old boy with pain demonstrates an obliquely oriented metaphyseal fracture (*black arrows*) and associated widening of the medial physis (*white arrow*) consistent with a Salter 2 fracture, (b) AP radiograph of the knee in a 15-year-old boy 2 weeks later demonstrates an obliquely oriented metaphyseal fracture (*black arrows*) with periosteal new bone formation along the distal shaft of the femur (*white arrowhead*) consistent with healing response

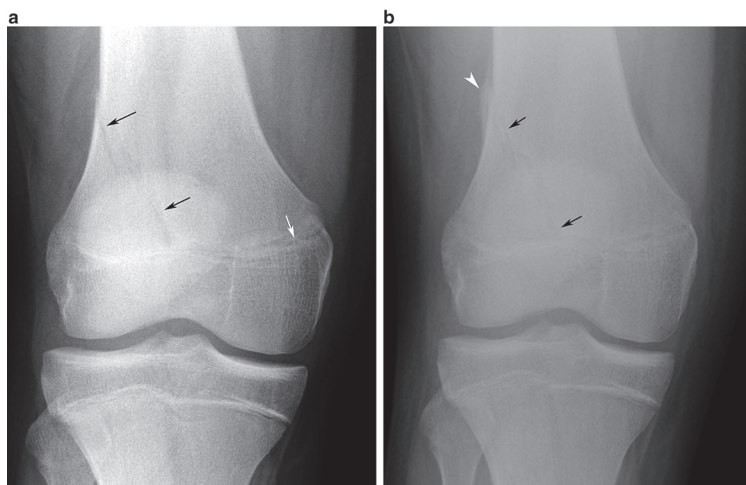
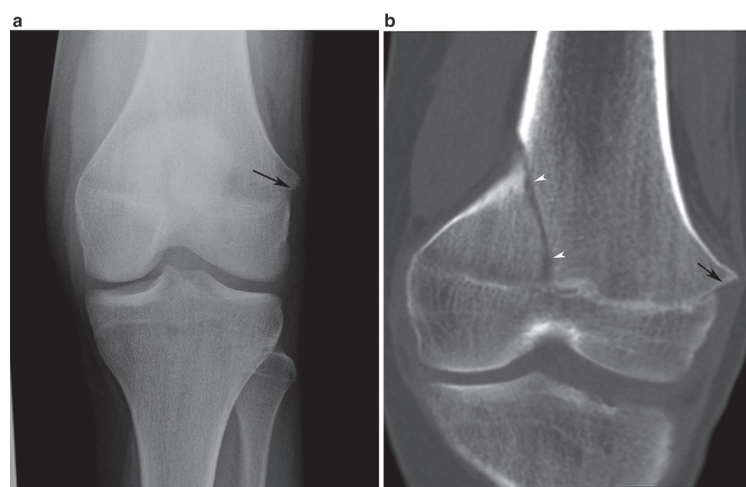


**Fig. 2.23** (a) AP radiograph of the knee in a 15-year-old female demonstrates a cortical stepoff along the lateral margin of the distal femur at the level of the physis (*black arrow*). No definite fracture lucency is appreciated. (b) Coronal reformatted image from a CT scan of the knee in a 15-year-old female demonstrates a metaphyseal fracture within the distal femur (*white arrowheads*) with widening of the physis and abnormal displacement of the lateral femoral condyle with respect to the metaphysis (*black arrow*), consistent with a Salter 2 fracture



## Avascular Necrosis

Avascular necrosis (AVN) is a debilitating complication of intra-capsular femoral neck fracture in 8.5–29.3% of patients, even after surgical intervention has been performed [49]. Avascular necrosis is caused by an alteration in the blood supply to the femoral head. Risk factors for the development of AVN are poorly understood, and include the severity of the initial injury, the time interval between injury and treatment, and type of treatment [50]. AVN is a late complication that may not develop until 18 months to 2 years after the fracture. The radiographic features of the condition demonstrate both the necrotizing and reparative processes that take place in the bone. Radiographs

are generally insensitive in the initial stages of osteonecrosis [51]. One of the earliest radiographic features of the disease process is a sclerotic epiphysis and/or a subchondral fissure, fracture, or focal collapse within a section of necrotic bone [51] (Figs. 2.36 and 2.37). This fissure is typically in the anterolateral epiphysis, best imaged with a frog-leg lateral radiograph. Bony resorption follows, with areas of mixed lucency on radiographs, followed by bone deposition and reconstitution of the bony outline [51] (Fig. 2.38).

Early on in the disease process, MRI imaging will demonstrate signal abnormalities within the anterosuperior portion of the femoral head with surrounding bands of dark signal on both T1- and T2-weighted images. MRI is limited, however, in



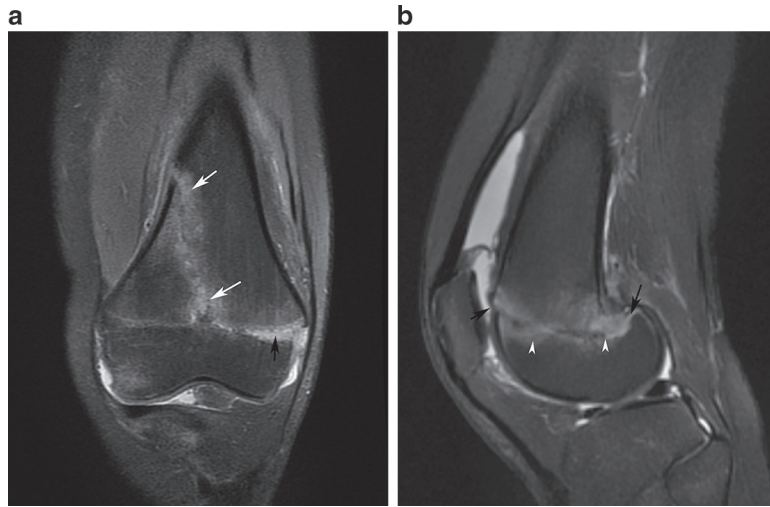


**Fig. 2.24** (a) Coronal PD-weighted image with fat-suppression through the knee in a 16-year-old female demonstrates a fracture line within the femoral metaphysis with surrounding marrow edema (*white arrows*) and abnormal fluid signal within a widened distal femoral physis (*black arrow*). (b) Sagittal T2-weighted image

with fat-suppression through the knee in a 16-year-old female demonstrates abnormal edema surrounding the distal femoral physis (*white arrowheads*) with mild posterior displacement of the femoral epiphysis with respect to the metaphysis (*black arrows*). There is also a moderate joint effusion



**Fig. 2.25** Sagittal T2-weighted image with fat-suppression through the knee in a 13-year-old female with no injury demonstrates the normal appearance of the bright signal within the distal femoral physis adjacent to the darker signal within the zone of provisional calcification

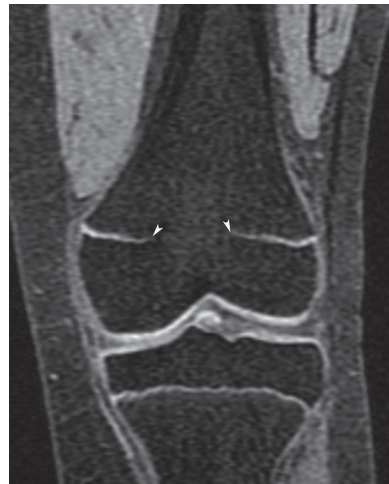


**Fig. 2.26** Coronal reformatted image from a 3D-MEDIC sequence through the knee in a 10-year-old girl demonstrates a central interruption of the otherwise bright distal femoral physis (*white arrowheads*) at the site of physeal bridge

its ability to predict which portions of the femoral head will revascularize and heal. Hyperintense signal in the femoral head on T2-weighted images can be a nonspecific finding in various

disease processes, which includes stress injury, infection, and osteopenia.

Currently, approaches to imaging remain relatively suboptimal for prediction of avascular



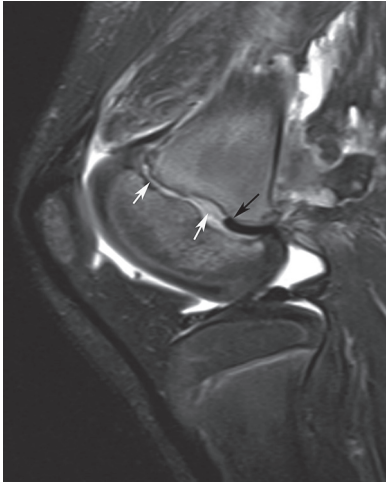


**Fig. 2.27** Sagittal T2-weighted image with fat-suppression through the knee in a 6-year-old male with a Salter 2 fracture demonstrates abnormal fluid signal within the physis (*white arrows*), and entrapment of the posterior periosteum within the physis (*black arrow*). There is also a joint effusion and soft tissue edema



**Fig. 2.28** Coronal PD-weighted image with fat-suppression through the knee in a 16-year-old male with a Salter 2 fracture demonstrates a low-signal subarticular fracture line (*white arrowheads*) within the lateral femoral condyle with surrounding marrow edema. Incidental note is made of a NOF within the proximal tibia

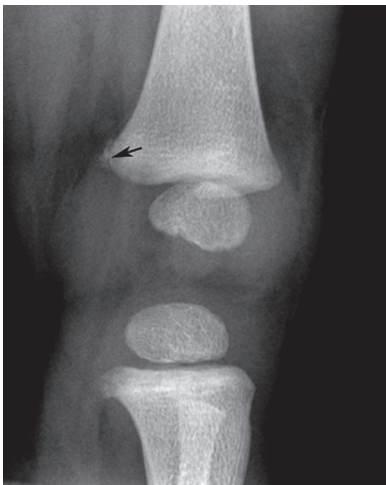


**Fig. 2.29** Oblique radiograph of the left knee in a 6-month-old male victim of abuse demonstrates an oblique lucency along the posterior margin of the metaphyseal/epiphyseal junction of the left distal femur (*black arrow*), consistent with a "corner fracture," or classic metaphyseal lesion (CML)

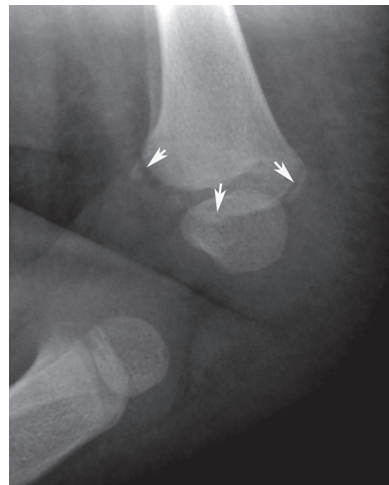


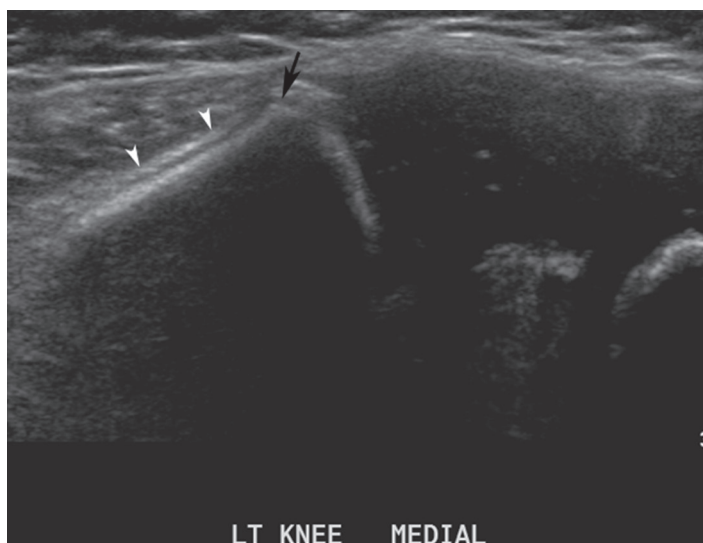
**Fig. 2.30** Lateral radiograph of the left knee in a 6-month-old male demonstrates a curvilinear lucency along the margin of the metaphyseal/epiphyseal junction of the left distal femur (*white arrows*) consistent with a "bucket-handle fracture," or classic metaphyseal lesion (CML)

necrosis before irreversible damage has occurred. Noncontrast enhanced MRI of the femoral head after acute femoral neck fracture is inadequate to determine the viability of the head and therefore a poor predictor of subsequent AVN [52]. In one study, bone scintigraphy with SPECT (single-photon emission computed tomography) was



**Fig. 2.31** AP radiograph of the left femur in a 7-year-old female victim of child abuse demonstrates abundant callous formation along the proximal femur (*black arrows*) and mild inferior displacement of the femoral head ossification center (*white arrowhead*) consistent with a healing fracture to the proximal femoral physis. A CML at the distal femur is also noted

**Fig. 2.32** Ultrasound image of the left knee in a 6-month-old female from a medial approach demonstrates early periosteal new bone formation along the distal shaft of the femur (*white arrowheads*). There is a small echolucent fracture line at the metaphyseal/epiphyseal junction (*black arrow*). Of note, the non-ossified femoral condyles appear dark given the lack of ossification



more sensitive than noncontrast MRI in detecting early osteonecrosis of the femoral heads after renal transplantation [53]. Decreased perfusion to the femoral head after femoral neck fracture manifests in bone scintigraphy as a cold defect in the femoral head (Fig. 2.39a, b). However, while nuclear medicine studies have been the gold standard in the assessment of the vascularity of the proximal femur where potential compromise to the blood supply has occurred, reduced uptake in the acute stage does not always correlate well with eventual development of AVN. A bone scan performed between 2 and 3 weeks post-injury may be used to assess epiphyseal vascularity [6]. MRI with contrast is helpful in assessing the enhancement pattern of the femoral head (Fig. 2.40a–c). Dynamic contrast-enhanced MRI is a technique that allows early detection of ischemic change in the hip [54]. This technique has replaced bone scintigraphy in many centers because of its ability to accurately depict femoral head deformity, cartilage and labral damage, and abnormalities of adjacent soft tissue structures in addition to the perfusion pattern of the femoral head. Reperfusion patterns of the hip are similar between dynamic gadolinium-enhanced subtraction MR imaging and bone scintigraphy in patients with Legg-Calve-Perthes disease (LCP), but have not been investigated extensively in patients with femoral fracture [55]. There is ongoing research investigating the utility

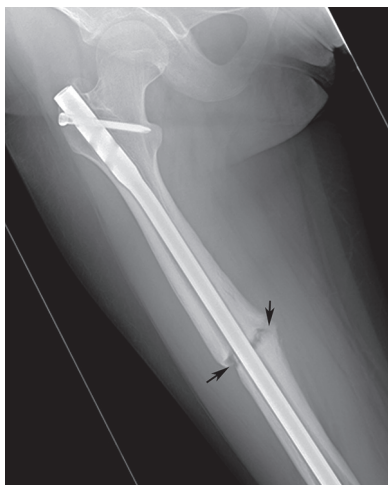


**Fig. 2.33** AP radiograph of the right femur in a 12-year-old female 1 year s/p fall demonstrates a hypertrophic nonunion (*black arrows*) despite placement of a rigid intramedullary nail across the fracture site. There is no cortical bridging across the callus, and the fracture line is still visible and irregular in contour

of diffusion-weighted imaging (DWI) in the hip to determine whether changes on diffusion-weighted images correlate with prognosis. DWI detects ischemic changes in tissues by measuring changes in water mobility. Diffusion-weighted imaging has been shown to detect early ischemia in the femoral head in a piglet model [56]. Preliminary studies on human patients with LCP demonstrated the presence of age-related diffusion changes in the femoral head, as well as the development of metaphyseal changes that suggest that DWI may have a future potential role in predicting prognosis [57, 58]. Although these methods have not been proven in pediatric patients with femoral neck fractures, dynamic MR perfusion imaging and diffusion-weighted imaging are likely to be promising techniques for predicting post-traumatic femoral head AVN with further investigation into their efficacy.

### Growth Disturbance/Leg Length Discrepancy

Leg length discrepancy is a potential complication of femoral fractures, particularly if the fracture involves the distal femoral growth plate. The

distal femoral physis contributes to approximately 50% of the overall length of the leg [22]. Growth disturbances occur when there has been significant damage to the epiphyseal plate or its blood supply, which may occur with any type of Salter-Harris fracture. Fractures in the proximal femur may lead to varus or valgus deformities depending on the location of the fracture and the pattern of healing (Fig. 2.41). Development of a leg length discrepancy is correlated with the degree of displacement and the quality of the reduction (whether open or closed) [21, 22]. The Salter-Harris classification of physeal fractures also provides an accurate predictor of outcome, with type V fractures requiring more reconstructive surgery to improve function than type I [22]. Growth arrest is usually appreciable within 12–18 months following post-injury [21]. Patients should therefore be followed closely for at least 1–2 years after an injury when the possibility of physeal disturbance exists [59].

An accurate method of measuring the amount of leg length discrepancy is a “scanogram” or “orthoroentgenogram” [60]. On a single film, three exposures are made with the beam centered successively over the hips, knees, and ankles. Two sliding metal shields allow an exposure to be made over one-third of the film while the remainder of the film is protected from exposure. A ruler may be placed at the side of the patient to facilitate accurate measurement of the leg length. Given that the focal spots are directly over each joint, there is no divergence of the beam and therefore no significant magnification of the resultant image. The total lengths of the femurs and tibia may be measured on each side to determine the difference between sides and is a reliable tool for pre-operative planning prior to epiphysiodesis, in which large threaded screws may be placed across the physis or drilling and curettage of the growth plate performed in order to halt the growth on one side of a long bone (Fig. 2.42a, b). Alternatively, a computerized tomography scanogram (CT-scanogram) may be performed utilizing a single AP scout image from the pelvis to the ankles, and acquiring a direct measurement from this image [61].

**Fig. 2.34** (a) AP radiograph of the right hip in a 15-year-old male s/p fall demonstrates a transcervical femoral neck fracture with medial angulation (*black arrow*) at the fracture site. (b, c) Reformatted coronal image from a CT scan of the hip in the same 15-year-old male 6 months s/p placement of three screws across the fracture site. The study was performed on a 64-detector CT scanner using metal reduction post-processing algorithm, allowing the fracture line to remain clearly seen (*black arrows*) secondary to the relatively minimal streak artifact related to the metal hardware

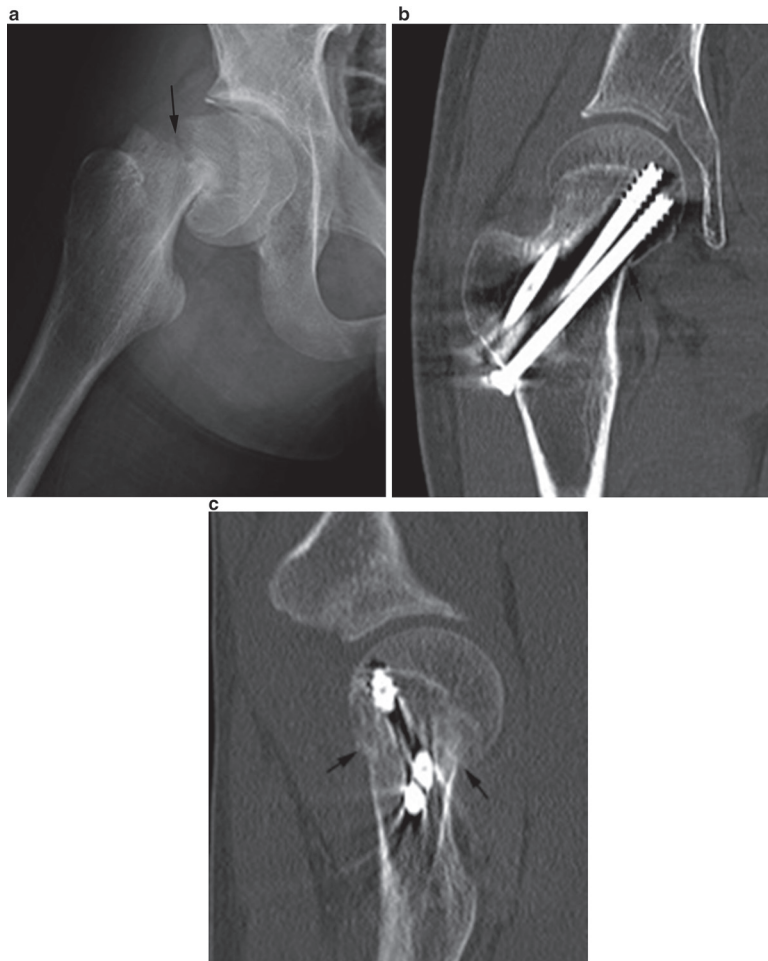


**Fig. 2.35** AP radiograph of the right femur in a 16-year-old male with an intramedullary rod and distal interlocking screw spanning a healing midshaft femur fracture demonstrates a crack in the interlocking screw (*black arrow*) and an angulation in the screw at the level of the discontinuity

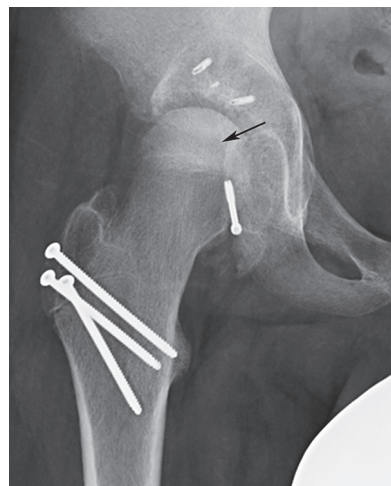


**Fig. 2.36** AP radiograph of the right hip in a 12-year-old male s/p MVA who suffered a dislocation/relocation injury to the right hip treated with surgical dislocation, screw fixation of Pipkin fracture, and posterior labral refixation/repair demonstrates a sclerotic femoral head (*black arrow*) consistent with development of AVN 4 months after injury



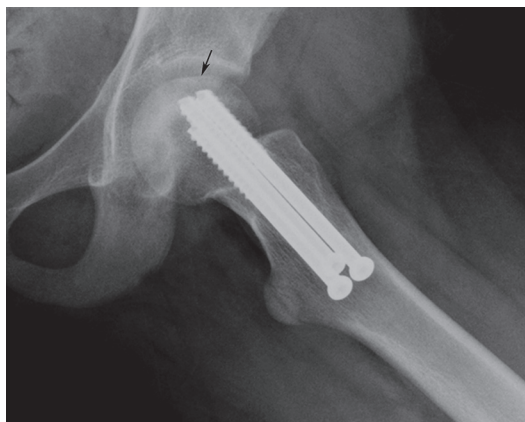


**Fig. 2.37** Frog-leg lateral radiograph of the left hip in a 12-year-old female 9 months s/p surgical repair of a femoral neck fracture with three femoral neck screws demonstrates early, subtle sclerosis within the head with mild flattening of the anterior femoral head contour associated with a subtle subchondral fissure (*black arrow*), representing early radiographic changes of AVN

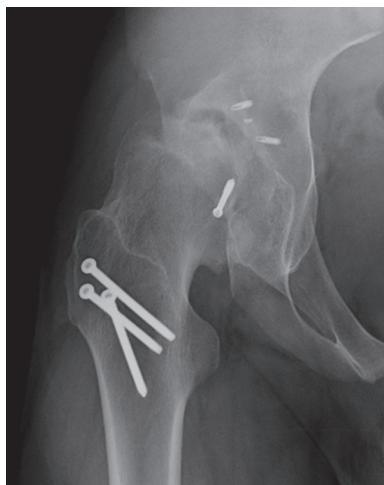


**Fig. 2.38** AP radiograph of the right hip in a 12-year-old male s/p MVA who suffered a dislocation/relocation injury to the right hip treated with surgical dislocation, screw fixation of Pipkin fracture, and posterior labral refixation/repair demonstrates a sclerotic femoral head (*black arrow*) consistent with progression to end-stage arthrosis secondary to AVN 16 months after injury

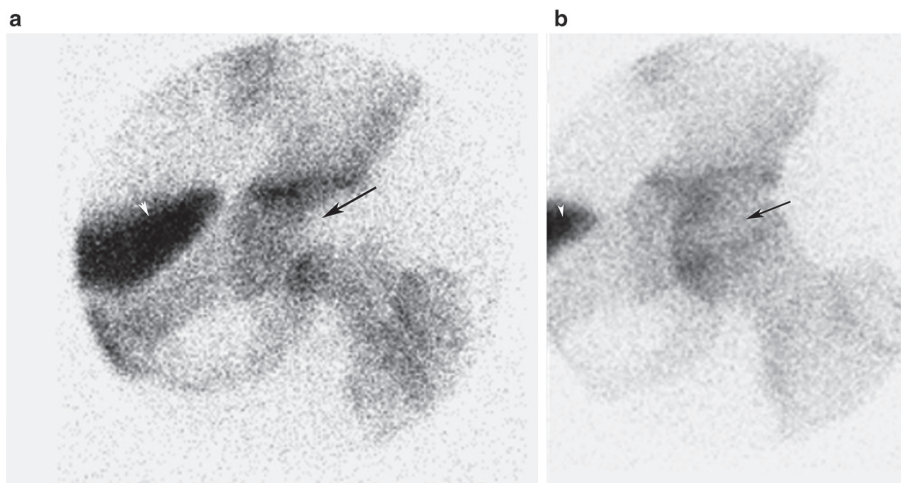


**Fig. 2.39** (a) AP pinhole collimated image of the left hip from a bone scintigraphy study on a 6-year-old patient 4 days s/p open reduction and internal fixation of the left hip for femoral neck fracture demonstrates no perfusion to the femoral head (*black arrow*). The *white arrowhead* denotes the bladder. (b) AP pinhole collimated image of the left

hip from a bone scintigraphy study on a 6-year-old patient 4 months s/p open reduction and internal fixation of the left hip for femoral neck fracture demonstrates improved perfusion to the femoral head (*black arrow*). The *white arrowhead* denotes the bladder

## Physeal Bridge

Though “scanograms” are well suited for evaluating the severity of a patient’s growth disturbance, they are not suited for evaluating bony

physeal bridges that directly contribute to the growth disturbance. The size and location of bony bridges are important factors for determining prognosis and indications for surgery. MRI is the preferred modality for evaluating such





**Fig. 2.40** (a) AP pelvis radiograph in a 16-year-old male s/p motorcycle accident demonstrates a comminuted left transcervical femoral neck fracture with mild angulation and a free fragment inferior to the neck (*black arrow*). (b, c) Coronal T1-weighted image without contrast through the

hips in the same patient one year after injury demonstrates flattening and sclerosis within the superior aspect of the femoral head (*black arrow*) representing an area of avascular necrosis. Post-surgical changes are noted within the femoral neck related to prior hardware placement and removal



**Fig. 2.41** AP pelvis radiograph in a 5-year-old female s/p bilateral proximal femoral physeal fractures in infancy, now with post-traumatic coxa vara deformities (*black arrows*)

physeal abnormalities. Fat-suppressed three-dimensional (3D) spoiled gradient-recalled echo (SPGR) sequences are very useful for identifying patterns of growth arrest in children after physeal insult due to high spatial resolution, multiplanar imaging capabilities, and excellent contrast between bone and cartilage signal [62–64]. Bony bridges are well visualized on 3D-SPGR sequences as a low-intensity zone within the physis, iso-intense to suppressed fatty marrow, and hypo-intense to the adjacent cartilaginous physis [62]. Maximum intensity projections (MIPs) of the juxtaphyseal area in the axial (transverse) plane allow mapping of the area of bony bridging and determination of the size of the bridge relative to the entire phy-

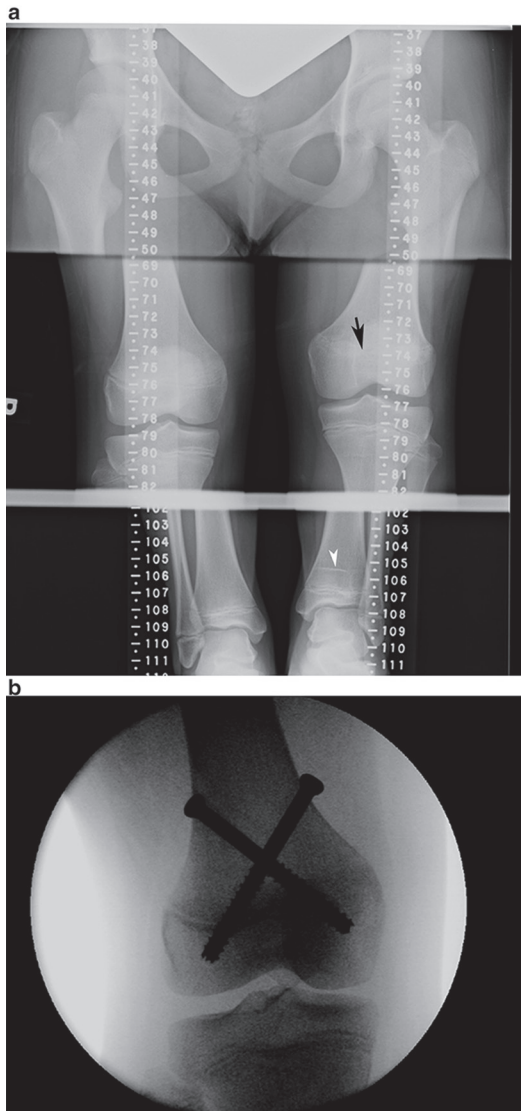


**Fig. 2.42** (a) Scanogram (orthoroentgenogram) on a 12-year-old female 18 months after sustaining a physal fracture to the left distal femur. The left distal femoral physis has fused (*black arrow*) earlier than the right side, and there is a nearly 2 cm leg length discrepancy. Incidental note is made of a growth recovery line in the distal left tibia (*white arrowhead*). (b) Fluoroscopic spot images from a screw epiphysiodesis in a 12-year-old female 18 months after sustaining a physal fracture to the left distal femur. Two cannulated screws were placed across the distal femoral physis of the right knee to correct for the growth disturbance on the left

sis (Fig. 2.43). On T1-weighted images the bone bridge demonstrates high signal intensity, unless the bridge is small in which case the signal may

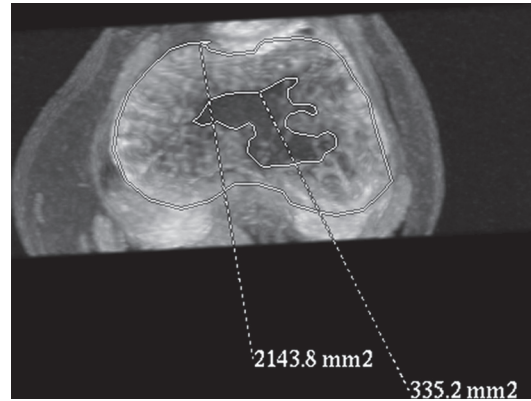


**Fig. 2.43** Axial maximum intensity projection (MIP) image from a 3D-SPGR sequence in the knee of an 11-year-old girl who sustained a Salter 2 fracture of the distal femur 7 months ago. The area of the physis and a central physal bone bridge were measured on a workstation, which reveal that the bone bridge spans ~15 % of the physis

be variable in intensity. The distal femoral physis is particularly vulnerable to premature physal bridging after trauma, likely related to a complex undulating pattern in the central physis corresponding to an area of early physiologic closure [65]. Growth recovery lines are also indicators of growth disturbance. Often identified as thin, linear sclerotic bands on radiographs in proximity to the physis, these bands are best visualized at MRI on T1-weighted images as low-intensity bands surrounded by high-intensity fatty marrow [62]. The orientation of the growth recovery line often serves as indicator as the location and size of the physal bridge. Peripheral bone bridges tend to be small and lead to tethered growth recovery lines that are angled relative to the physis [62]. Central bony bridges produce growth recovery lines parallel to the physis, and are of variable size.

## Infection

Infection is an uncommon complication of femur fractures. Imaging rarely plays a significant role in patients with early wound infections after surgery, as it takes at least 2 weeks for radiographic features of infection to manifest. Abnormal and

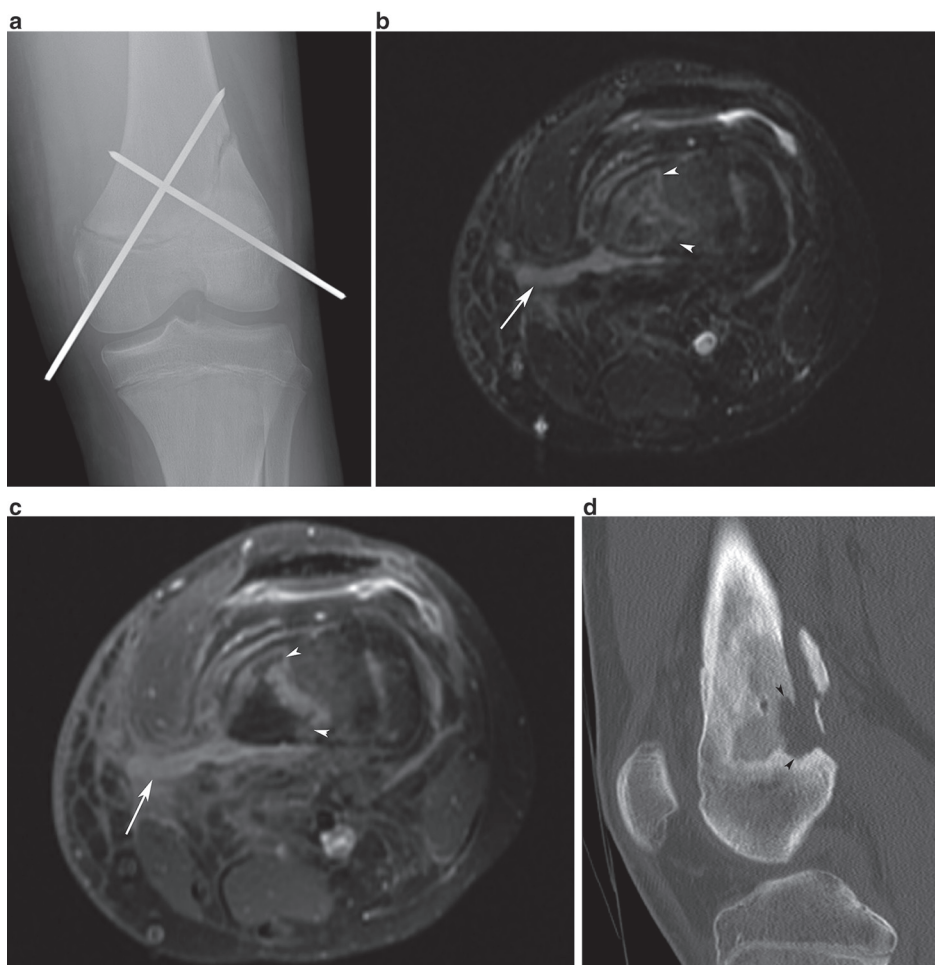


**Fig. 2.44** (a) AP radiograph of the knee in a 15-year-old male s/p Salter 2 fracture demonstrates two K wires spanning the fracture through the distal femur and physis. (b) Axial T2-weighted fat-suppressed image through the knee in the same 15-year-old patient 3 weeks after surgery. The pins were removed because they became exposed. MRI reveals an area of signal abnormality within the distal femur (*white arrowheads*) and a bright tract extending from the bone to the subcutaneous soft tissues (*white arrow*), representing an area of infection. (c) Axial T1-weighted, post-contrast, fat-suppressed image through

the knee in the same 15-year-old patient 3 weeks after surgery reveals a rim-enhancing area of signal abnormality within the distal femur (*white arrowheads*) consistent with an intra-osseous abscess, and an enhancing tract extending from the bone to the subcutaneous soft tissues (*white arrow*), representing a draining sinus. (d) Corresponding sagittal reformatted image from a CT scan through the knee in the same 15-year-old patient 3 weeks after surgery reveals an area of low attenuation within the distal femur and focal bony destruction (*black arrowheads*) corresponding to the abscess detected at MRI

increasing lucency around metallic hardware is one early radiographic sign of infection, but may also be seen in the setting of hardware loosening.

Sonography may be useful to evaluate for soft tissue infection adjacent to orthopedic devices, including soft tissue abscess and bursitis, but is not as useful for imaging the bone. CT and MRI imaging better demonstrate bone detail

(Fig. 2.44a–d). Imaging a post-operative orthopedic patient with cross-sectional imaging may be challenging given the artifacts associated with most implants at CT and MRI. These artifacts, however, are becoming increasingly easier to manage with advances in imaging technology. Titanium implants result in the least amount of CT and MR artifact [66]. Artifact may be further reduced at CT by careful positioning of the

patient in the scanner, and meticulous post-processing algorithms. Faster MRI imaging techniques have resulted in decreased metal artifacts relative, and wider readout bandwidths may be employed to reduce metal artifact [66].

CT imaging findings of infection in a patient with hardware include periosteal reaction, areas of focal lucency, sequestra, areas of bone sclerosis, and soft tissue fluid collections [47]. These findings, however, are not specific for infection. At MRI areas of abnormal bright signal on fluid-sensitive sequences surrounding hardware and fracture sites may indicate possible infection, but these findings are nonspecific. 18F-FDG PET/CT imaging combines the anatomic localization of CT with functional PET imaging, and is the first line cross-sectional imaging study in patients with suspected spinal hardware infection [67]. This technique may also be useful in a patient with a suspected hardware infection after femur fracture, and provides greater specificity for infection than CT alone.

## References

1. Eliahou R, Simanovsky N, Hiller N, Simanovsky N. Fracture-separation of the distal femoral epiphysis in a premature neonate. *J Ultrasound Med*. 2006;25(12):1603–5. Epub 2006/11/24.
2. Bennett FS, Zinar DM, Kilgus DJ. Ipsilateral hip and femoral shaft fractures. *Clin Orthop Relat Res*. 1993;296:168–77. Epub 1993/11/01.
3. Dimeglio A. Growth in pediatric orthopaedics. *J Pediatr Orthop*. 2001;21(4):549–55. Epub 2001/07/04.
4. Beaty JH, Kasser JR. Rockwood and Wilkins' fractures in children. Philadelphia: Wolters Kluwer/Lippincott, Williams & Wilkins; 2010.
5. Vialle R, Odent T, Pannier S, Pauthier F, Laumonier F, Glorion C. Traumatic hip dislocation in childhood. *J Pediatr Orthop*. 2005;25(2):138–44. Epub 2005/02/19.
6. Vialle R, Pannier S, Odent T, Schmit P, Pauthier F, Glorion C. Imaging of traumatic dislocation of the hip in childhood. *Pediatr Radiol*. 2004;34(12):970–9. Epub 2004/09/28.
7. Stewart MJ, Milford LW. Fracture-dislocation of the hip; an end-result study. *J Bone Joint Surg Am*. 1954;36(A:2):315–42. Epub 1954/04/01.
8. Pipkin G. Treatment of grade IV fracture-dislocation of the hip. *J Bone Joint Surg Am*. 1957;39-A(5):1027–42. passim. Epub 1957/10/01.
9. DeBC PC. Fractures of the neck of the femur in children. *Am J Surg*. 1929;6:793–7.
10. Moon ES, Mehlman CT. Risk factors for avascular necrosis after femoral neck fractures in children: 25 Cincinnati cases and meta-analysis of 360 cases. *J Orthop Trauma*. 2006;20(5):323–9. Epub 2006/06/13.
11. Hakkarinen DK, Banh KV, Hendey GW. Magnetic resonance imaging identifies occult hip fractures missed by 64-slice computed tomography. *J Emerg Med*. 2012;43(2):303–7. Epub 2012/03/31.
12. Rubel IF, Kloen P, Potter HG, Helfet DL. MRI assessment of the posterior acetabular wall fracture in traumatic dislocation of the hip in children. *Pediatr Radiol*. 2002;32(6):435–9. Epub 2002/05/25.
13. Novais EN, Millis MB. Slipped capital femoral epiphysis: prevalence, pathogenesis, and natural history. *Clin Orthop Relat Res*. 2012;470(12):3432–8. Epub 2012/10/12.
14. Elmadag M, Ceylan HH, Erdem AC, Bilsel K, Uzer G, Acar MA. Pediatric transepiphyseal separation and dislocation of the femoral head. *Case Rep Orthop*. 2013;2013:703850. Epub 2013/04/11.
15. Cannon SR, Pool CJ. Traumatic separation of the proximal femoral epiphysis and fracture of the mid-shaft of the ipsilateral femur in a child. A case report and review of the literature. *Injury*. 1983;15(3):156–8. Epub 1983/11/01.
16. Vangsness Jr CT, DeCampos J, Merritt PO, Wiss DA. Meniscal injury associated with femoral shaft fractures. An arthroscopic evaluation of incidence. *J Bone Joint Surg Br*. 1993;75(2):207–9. Epub 1993/03/01.
17. Letts M, Vincent N, Gouw G. The “floating knee” in children. *J Bone Joint Surg Br*. 1986;68(3):442–6. Epub 1986/05/01.
18. Chauvin N, Jaramillo D. Occult distal femoral physeal injury with disruption of the perichondrium. *J Comput Assist Tomogr*. 2012;36(3):310–2. Epub 2012/05/18.
19. Salter RB, HR. Injuries involving the epiphyseal plate. *J Bone Joint Surg Am*. 1963;45(3):587–622.
20. Lippert WC, Owens RF, Wall EJ. Salter-Harris type III fractures of the distal femur: plain radiographs can be deceptive. *J Pediatr Orthop*. 2010;30(6):598–605. Epub 2010/08/25.
21. Lombardo SJ, Harvey Jr JP. Fractures of the distal femoral epiphyses. Factors influencing prognosis: a review of thirty-four cases. *J Bone Joint Surg Am*. 1977;59(6):742–51. Epub 1977/09/01.
22. Czitrom AA, Salter RB, Willis RB. Fractures involving the distal epiphyseal plate of the femur. *Int Orthop*. 1981;4(4):269–77. Epub 1981/01/01.
23. Bali K, Mootha AK, Prabhakar S, Dhillon MS. Isolated Hoffa fracture of the medial femoral condyle in a skeletally immature patient. *Bull NYU Hosp Jt Dis*. 2011;69(4):335–8. Epub 2011/12/27.
24. Smith BG, Rand F, Jaramillo D, Shapiro F. Early MR imaging of lower-extremity physeal fracture-separations: a preliminary report. *J Pediatr Orthop*. 1994;14(4):526–33. Epub 1994/07/01.
25. Close BJ, Strouse PJ. MR of physeal fractures of the adolescent knee. *Pediatr Radiol*. 2000;30(11):756–62. Epub 2000/12/02.



26. Ogden JA. Injury to the growth mechanisms of the immature skeleton. *Skeletal Radiol.* 1981;6(4):237–53. Epub 1981/01/01.
27. Vellet AD, Marks PH, Fowler PJ, Munro TG. Occult posttraumatic osteochondral lesions of the knee: prevalence, classification, and short-term sequelae evaluated with MR imaging. *Radiology.* 1991;178(1):271–6. Epub 1991/01/01.
28. Naranja Jr RJ, Gregg JR, Dormans JP, Drummond DS, Davidson RS, Hahn M. Pediatric fracture without radiographic abnormality. Description and significance. *Clin Orthop Relat Res.* 1997;342:141–6. Epub 1997/10/06.
29. Clarke NM, Shelton FR, Taylor CC, Khan T, Needhirajan S. The incidence of fractures in children under the age of 24 months—in relation to non-accidental injury. *Injury.* 2012;43(6):762–5. Epub 2011/09/23.
30. Worlock P, Stower M, Barbor P. Patterns of fractures in accidental and non-accidental injury in children: a comparative study. *Br Med J (Clin Res Ed).* 1986;293(6539):100–2. Epub 1986/07/12.
31. Akbarnia B, Torg JS, Kirkpatrick J, Sussman S. Manifestations of the battered-child syndrome. *J Bone Joint Surg Am.* 1974;56(6):1159–66. Epub 1974/09/01.
32. Pandya NK, Baldwin K, Wolfgruber H, Christian CW, Drummond DS, Hosalkar HS. Child abuse and orthopaedic injury patterns: analysis at a level I pediatric trauma center. *J Pediatr Orthop.* 2009;29(6):618–25. Epub 2009/08/25.
33. Kleinman PK, Marks SC, Blackburne B. The metaphyseal lesion in abused infants: a radiologic-histopathologic study. *Am J Roentgenol.* 1986;146(5):895–905. Epub 1986/05/01.
34. Caffey J. Some traumatic lesions in growing bones other than fractures and dislocations: clinical and radiological features: The Mackenzie Davidson Memorial Lecture. *Br J Radiol.* 1957;30(353):225–38. Epub 1957/05/01.
35. Kleinman PK, Perez-Rossello JM, Newton AW, Feldman HA, Kleinman PL. Prevalence of the classic metaphyseal lesion in infants at low versus high risk for abuse. *Am J Roentgenol.* 2011;197(4):1005–8. Epub 2011/09/24.
36. Kleinman PK, Marks Jr SC. A regional approach to the classic metaphyseal lesion in abused infants: the proximal tibia. *Am J Roentgenol.* 1996;166(2):421–6. Epub 1996/02/01.
37. Kleinman PK. *Diagnostic imaging of child abuse.* 2nd ed. St. Louis, MO: Mosby; 1998.
38. Chintalapani G, Ellingsen LM, Sadowsky O, Prince JL, Taylor RH. Statistical atlases of bone anatomy: construction, iterative improvement and validation. *Med Image Comput Assist Interv.* 2007;10(Pt 1):499–506. Epub 2007/12/07.
39. Shrader MW, Stans AA, Shaughnessy WJ, Haidukewych GJ. Nonunion of fractures in pediatric patients: 15-year experience at a level I trauma center. *Orthopedics.* 2009;32(6):410. Epub 2009/07/29.
40. Bhandari M, Guyatt GH, Swiontkowski MF, Tornetta III P, Sprague S, Schemitsch EH. A lack of consensus in the assessment of fracture healing among orthopaedic surgeons. *J Orthop Trauma.* 2002;16(8):562–6. Epub 2002/09/28.
41. Morshed S, Corrales L, Genant H, Miclau III T. Outcome assessment in clinical trials of fracture-healing. *J Bone Joint Surg Am.* 2008;90 Suppl 1:62–7. Epub 2008/03/20.
42. Whelan DB, Bhandari M, McKee MD, Guyatt GH, Kreder HJ, Stephen D, et al. Interobserver and intraobserver variation in the assessment of the healing of tibial fractures after intramedullary fixation. *J Bone Joint Surg Br.* 2002;84(1):15–8. Epub 2002/02/12.
43. Panjabi MM, Walter SD, Karuda M, White AA, Lawson JP. Correlations of radiographic analysis of healing fractures with strength: a statistical analysis of experimental osteotomies. *J Orthop Res.* 1985;3(2):212–8. Epub 1985/01/01.
44. Blokhuis TJ, de Bruijn JH, Bramer JA, den Boer FC, Bakker FC, Patka P, et al. The reliability of plain radiography in experimental fracture healing. *Skeletal Radiol.* 2001;30(3):151–6. Epub 2001/05/19.
45. Vande Berg B, Malghem J, Maldague B, Lecouvet F. Multi-detector CT imaging in the postoperative orthopedic patient with metal hardware. *Eur J Radiol.* 2006;60(3):470–9. Epub 2006/11/03.
46. Kalender WA, Hebel R, Ebersberger J. Reduction of CT artifacts caused by metallic implants. *Radiology.* 1987;164(2):576–7. Epub 1987/08/01.
47. Ohashi K, El-Khoury GY, Bennett DL, Restrepo JM, Berbaum KS. Orthopedic hardware complications diagnosed with multi-detector row CT. *Radiology.* 2005;237(2):570–7. Epub 2005/10/26.
48. Fayad LM, Patra A, Fishman EK. Value of 3D CT in defining skeletal complications of orthopedic hardware in the postoperative patient. *Am J Roentgenol.* 2009;193(4):1155–63. Epub 2009/09/23.
49. Bachiller FG, Caballer AP, Portal LF. Avascular necrosis of the femoral head after femoral neck fracture. *Clin Orthop Relat Res.* 2002;399:87–109. Epub 2002/05/16.
50. Hajdu S, Oberleitner G, Schwendenwein E, Ringl H, Vecsei V. Fractures of the head and neck of the femur in children: an outcome study. *Int Orthop.* 2011;35(6):883–8. Epub 2010/05/22.
51. Ozonoff MB. *Pediatric orthopedic radiology.* 2nd ed. Philadelphia, PA: W.B. Saunders, Co.; 1992.
52. Speer KP, Spritzer CE, Harelson JM, Nunley JA. Magnetic resonance imaging of the femoral head after acute intracapsular fracture of the femoral neck. *J Bone Joint Surg Am.* 1990;72(1):98–103. Epub 1990/01/01.
53. Ryu JS, Kim JS, Moon DH, Kim SM, Shin MJ, Chang JS, et al. Bone SPECT is more sensitive than MRI in the detection of early osteonecrosis of the femoral



- head after renal transplantation. *J Nucl Med.* 2002;43(8):1006–11. Epub 2002/08/07.
54. Sebag G, Ducou Le Pointe H, Klein I, Maiza D, Mazda K, Bensahel H, et al. Dynamic gadolinium-enhanced subtraction MR imaging—a simple technique for the early diagnosis of Legg-Calve-Perthes disease: preliminary results. *Pediatr Radiol.* 1997;27(3):216–20. Epub 1997/03/01.
  55. Lamer S, Dorgeret S, Khairouni A, Mazda K, Brillet PY, Bacheville E, et al. Femoral head vascularisation in Legg-Calve-Perthes disease: comparison of dynamic gadolinium-enhanced subtraction MRI with bone scintigraphy. *Pediatr Radiol.* 2002;32(8):580–5. Epub 2002/07/24.
  56. Menezes NM, Connolly SA, Shapiro F, Olear EA, Jimenez RM, Zurakowski D, et al. Early ischemia in growing piglet skeleton: MR diffusion and perfusion imaging. *Radiology.* 2007;242(1):129–36. Epub 2006/12/23.
  57. Yoo WJ, Kim YJ, Menezes NM, Cheon JE, Jaramillo D. Diffusion-weighted MRI reveals epiphyseal and metaphyseal abnormalities in Legg-Calve-Perthes disease: a pilot study. *Clin Orthop Relat Res.* 2011;469(10):2881–8. Epub 2011/06/11.
  58. Merlini L, Combescure C, De Rosa V, Anooshiravani M, Hanquinet S. Diffusion-weighted imaging findings in Perthes disease with dynamic gadolinium-enhanced subtracted (DGS) MR correlation: a preliminary study. *Pediatr Radiol.* 2010;40(3):318–25. Epub 2010/01/07.
  59. Skaggs DL. Extra-articular injuries of the knee. 6th ed. Beaty JH, Kasser, JR, editor. Philadelphia, PA: Lippincott, Williams, and Wilkins; 2006. p. 937–84.
  60. Green WT, Wyatt GM, Anderson M. Orthoroentgenography as a method of measuring the bones of the lower extremities. *J Bone Joint Surg Am.* 1946;28:60–5. Epub 1946/01/01.
  61. Kogutt MS. Computed radiographic imaging: use in low-dose leg length radiography. *Am J Roentgenol.* 1987;148(6):1205–6. Epub 1987/06/01.
  62. Ecklund K, Jaramillo D. Patterns of premature physeal arrest: MR imaging of 111 children. *Am J Roentgenol.* 2002;178(4):967–72. Epub 2002/03/22.
  63. Borsa JJ, Peterson HA, Ehman RL. MR imaging of physeal bars. *Radiology.* 1996;199(3):683–7. Epub 1996/06/01.
  64. Sailhan F, Chotel F, Guibal AL, Gollogly S, Adam P, Berard J, et al. Three-dimensional MR imaging in the assessment of physeal growth arrest. *Eur Radiol.* 2004;14(9):1600–8. Epub 2004/04/06.
  65. Harcke HT, Synder M, Caro PA, Bowen JR. Growth plate of the normal knee: evaluation with MR imaging. *Radiology.* 1992;183(1):119–23. Epub 1992/04/01.
  66. Sofka CM, Potter HG, Adler RS, Pavlov H. Musculoskeletal imaging update: current applications of advanced imaging techniques to evaluate the early and long-term complications of patients with orthopedic implants. *HSS J.* 2006;2(1):73–7. Epub 2008/08/30.
  67. Bagrosky BM, Hayes KL, Koo PJ, Fenton LZ. (18) F-FDG PET/CT evaluation of children and young adults with suspected spinal fusion hardware infection. *Pediatr Radiol.* 2013;43(8):991–1000. Epub 2013/03/05.

Antibiotics

Methods and Protocols

Sass, P. (Ed.)

2017, XI, 358 p. 78 illus., 21 illus. in color., Hardcover

ISBN: 978-1-4939-6632-5

A product of Humana Press